

Beyond Price Taker: Conceptual Design and Optimization of Integrated Energy Systems using Machine Learning Market Surrogates

Jordan Jalving^{1,6}, Jaffer Ghouse^{2,3}, Nicole Cortes⁴, Xian Gao⁴, Bernard Knueven⁵, Damian Agi⁴, Shawn Martin¹, Xinhe Chen⁴, Darice Guittet⁵, Radhakrishna Tumbalam-Gooty^{2,3}, Ludovico Bianchi⁷, Keith Beattie⁷, Daniel Gunter⁷, John D. Sirola¹, David C. Miller², Alexander W. Dowling^{4*}

¹*Sandia National Laboratories, Albuquerque, NM 87123*

²*National Energy Technology Laboratory, Pittsburgh, PA 15236*

³*NETL Support Contractor, Pittsburgh, PA 15236*

⁴*Department of Chemical and Biomolecular Engineering
University of Notre Dame, Notre Dame, IN 46556*

⁵*National Renewable Energy Technology Laboratory, Golden, CO 80401*

⁶*Pasteur Labs, Brooklyn, NY 11205*

⁷*Lawrence Berkeley National Laboratory, Berkeley CA 94720*

Abstract

Future electricity generation systems must be optimized to provide flexibility that counteracts the variability of non-dispatchable renewable energy sources and ensures the reliability and safety of critical infrastructure, including the electric grid. The current state-of-the-art is to co-optimize the design and operation of integrated energy systems (IESs) treating historical or predicted time-series electricity prices as fixed parameters. Recent literature has shown the limitations of this price taker assumption, which neglects how IES optimization decisions influence market outcomes. As such, this paper proposes a new optimization formulation that uses machine learning surrogate models, training for a library of annual market operation simulations, to embed IES market interactions into the co-optimization problem directly. Using a thermal generator example built in the open-source IDAES computational environment, we show that the price taker approach routinely over-predicts

*Corresponding author

Email address: adowling@nd.edu (Alexander W. Dowling⁴)

JJ was formerly at Sandia National Laboratories. JG was formerly at the National Energy Technology Laboratory (KeyLogic).

annual revenues by 8% or more compared to a validation simulation, where the proposed approach has a typical relative error of 1% or less.

Highlights:

- Multiscale simulations reveal complex interactions between IESs and energy markets
- Standard price taker formulations are not predictive in realistic design scenarios
- Neural network surrogates accurately predict IES/market interactions
- Optimization with market surrogates is tractable and accurate
- Computational design framework is built entirely from open-source tools

Keywords: integrated energy systems, surrogate modeling, neural networks, electricity markets, energy infrastructure, computational optimization

1. Introduction

Integrated Energy Systems (IES) combine diverse energy sources (e.g., renewables, fossil, nuclear) in hybrid configurations to provide a mix of energy services (e.g., electricity, heat, steam, chemicals) while enabling the dynamic flexibility needed to incorporate non-dispatchable variable renewable energy sources into the electric grid and other energy infrastructure. This dynamic flexibility is critical for curtailing emissions, reducing costs, and ultimately meeting global deep-decarbonization goals while maintaining grid reliability and resiliency. However, IES design, operation, and control are inherently interrelated, multiscale engineering optimization problems. Globally, the economics of electricity generators are determined by interactions with wholesale energy markets, which span minutes (real-time markets), hours to days (day-ahead markets), and months to years (capacity markets). The current state-of-the-art is to formulate multiscale multiperiod optimization problems using time-series price forecasts for energy and other products (e.g., ancillary services) from historical data or other models. Per the price taker assumption, these prices are treated as fixed parameters and not impacted by the IES optimization decisions. Recent studies suggest the price taker assumption is invalid for flexible IESs in modern electricity markets with modest renewable penetration.

This paper proposes a novel multiscale IES optimization framework that explicitly incorporates exogenous uncertainty from market interactions as an alternative to the ubiquitous price taker assumption. From a library of over 64,000 annual market simulations, we train algebraic basis function and neural network surrogate models to accurately predict the revenue and dispatch of an IES as

a function of its design and market bid characteristics. We then formulate the conceptual design and operation of the IES as a two-stage stochastic program using the surrogate models to explicitly incorporate IES market interactions (i.e., exogenous uncertainty). Thus, our proposed formulation is a tractable representation of an otherwise multiscale, non-convex, and high-dimensional optimization problem. Using a thermal generator example built in the IDAES computational environment with rigorous nonlinear thermodynamics models, we show that our approach overcomes the price taker assumptions' limitations using annual market operation simulation for validation. Compared to the literature, the key contributions of this work are the surrogate models and companion IES optimization formulations that go beyond the price taker and self-schedule assumptions and their inherent limitations.

The manuscript is organized as follows: Section 2 presents detailed literature to contextualize the elements of the modeling framework. Section 3 discusses the underlying methods of the framework, which are divided into several key steps, including production cost modeling, training market surrogates, and formulating design optimization problems with the market surrogates embedded. Section 4 presents a comprehensive case study that replaces a thermal generator within a representative test power grid and benchmarks the price taker and our proposed market-surrogate approach. Section 5 summarizes the paper's key contributions and presents a future outlook on approaching IES design.

2. Literature Review

2.1. Wholesale energy markets set the time-varying value of electricity

Decarbonizing the electric grid and other energy infrastructure is critical to meet urgent and ambitious goals (e.g., the Paris Climate Accords) to protect the environment and mitigate climate change. In 2019, wind and photovoltaic (PV) solar accounted for 80% of the global energy supply growth [1]. However, to realize the massive adoption of non-dispatchable variable renewable energy sources (VREs) challenges such as high capital investment costs, the inability to accurately predict power output, and the inability to match periods of high power output to periods of high demand [2] still need to be addressed. In addition, increased renewable generation adoption has coincided with high curtailment rates, with some countries reaching up to 10% of their generation being curtailed or limited when supply outweighs demand [3]. In many countries, wholesale electricity

markets coordinate the generation and consumption of electricity and set prices in a two-settlement system: a day-ahead market to meet forecasted demand and a balancing real-time market for fast adjustments [4]. In the U.S., energy generation is scheduled by independent service operators (ISOs) who accept bids from market participants and then clear the market, often from lowest to higher cost, constrained by transmission limitations and spatiotemporal demands [5]. These market clearing processes set the locational marginal prices (LMPs), which determine the payments made and received by electricity consumers and producers, respectively. The benefits of VREs include zero dependence on fossil fuels and low or even zero production costs, which may decrease LMPs over time. Moreover, the stochastic nature of non-dispatchable VRE production also adds more uncertainty to market operations creating higher LMP volatility. The electric grid (and other energy infrastructure) need more dynamic flexibility to mitigate this volatility and incorporate more VREs while maintaining reliability and resiliency and reducing emissions [6, 7].

Integrated energy systems (IES) couple multiple energy technologies such as renewables, nuclear, fossil with carbon capture, energy storage, and flexible industrial systems to exploit the synergies among the processes and produce energy and (chemical) products more efficiently [8, 9]. Prior work has shown that integrating multiple energy technologies, such as energy storage, can increase the VRE capacity added to the grid while maintaining reliability [10]. Also, by better utilizing (waste) thermal energy, IESs have increased energy efficiency, decreased emissions, and help meet carbon emissions targets [11, 12, 13]. Due to the high value placed on the flexibility of these systems, models that capture the inherently dynamic nature of the modern electricity market are needed to conduct techno-economic analysis (TEA) on IES concepts properly [14, 15, 16, 9]. As an alternative to directly participating in wholesale energy markets, IES or prosumers can provide flexibility through demand response programs.[17]. Nevertheless, because wholesale energy markets set the underlying time-varying value of electricity, we focus on participation in these markets and leave consideration of demand response as future work.

2.2. Uncertain and time-varying prices necessitate optimization-based techno-economic analysis

The current state-of-the-art to evaluate the economic viability of IES concepts is to solve (multiscale) multiperiod optimization problems that model IES-grid interactions using the self-schedule and price taker assumptions, which go beyond the conventional TEA analysis that assumes a fixed price for electricity and a constant capacity factor to estimate a levelized cost of electricity (LCOE)

[18]. When an energy resource self-schedules, it submits a fixed schedule to the market operator and agrees to accept the final settled LMPs. Likewise, the price taker assumption is that the market participant is sufficiently small such that its actions will not influence market outcomes such as LMPs or dispatch schedules. These assumptions make it easy to use historical LMPs to estimate the maximum obtainable revenue from an IES optimally participating in one or more markets, as pioneered by Walawalkar et al. [19].

Optimization-based TEA using the price taker and self-schedule assumptions has become the de facto standard for IESs. As a recent example, Zantye and colleagues [13] utilized a multi-stage stochastic programming approach to optimally self-schedule a power generator with a flexible carbon capture unit. Flexible operation of the carbon capture unit allows the generator to increase power output during periods with high electricity prices and devote more energy to carbon capture during periods with lower electricity prices. In comparison to a deterministic model, their proposed approach yielded a value of the stochastic solution (VSS) of \$41,145, or a 40% improvement of the profit, indicating the value of accounting for uncertainty in next-day market clearing prices in the decision-making process. Jabari et al. [20] self-scheduled a combined water and power producer using a robust mixed-integer nonlinear programming (MINLP) model. Uncertain electricity price forecasts are first used to solve a deterministic optimization problem, then a set of stochastic price scenarios are used to solve a risk-averse robust problem. They also utilized a budget-of-uncertainty-parameter between 0 and 1 to represent the fraction of uncertain electricity prices in the time horizon. Their case studies showed that the robust approach allowed decision-makers to adjust model conservatism and generate risk-averse schedules. Attarha et al. [21] investigated the self-scheduling of a wind power producer with integrated compressed air energy storage. Specifically, they compared a deterministic and robust mixed-integer linear programming (MILP) model where the robust model considered uncertainty in wind power production and electricity price. They were able to conduct an after-the-fact analysis to quantify the long-term benefits of considering robustness in their model. Their results also highlighted that pairing compressed air energy storage with wind power production provided flexibility benefits over operating a wind farm alone. Bischi et al. [22] used a rolling-horizon algorithm to solve a MILP scheduling model for a cogeneration system. The rolling horizon algorithm allowed the model to consider yearly-basis energy-saving indexes to capture economic incentives in the optimization properly. Their formulation found an improved objective function versus standard weekly scheduling models and reduced operating costs

of up to 10% with proper incentives.

There is a growing consensus in the literature that energy storage systems must do more than just energy arbitrage in the wholesale electricity market to be profitable. For example, Fares and Webber [23] utilized self-schedule optimization models to demonstrate that battery technologies cannot make up their cost purely by participating in traditional energy arbitrage. They used a nonlinear programming problem to model lithium-ion batteries buying and selling in 15-minute increments. A related study considers dynamic self-schedule optimization of vanadium redox flow batteries for frequency regulation, resulting in similar findings about the importance of faster timescales [24]. Subsequent studies by Dowling and colleagues verified this finding — IESs such as batteries [15, 25, 26], cogeneration [15], concentrated solar power [18, 27], and energy-intensive industries [28, 29] should transact multiple market products at multiple timescales, and the fastest timescales are the most profitable when using the self-schedule and price taker assumptions. Likewise, a 2016 National Renewable Energy Technology Laboratory report [30] presents the application of a price taker optimization to assess the economic viability of hydrogen energy storage systems to participate in California’s wholesale electricity market. They found that producing and selling hydrogen gas was more profitable than storing it for later electricity production and that participation on multiple market timescales makes for higher revenue. Thus, this literature demonstrates the versatility of multiperiod optimization to estimate market revenues for IES participating in idealized markets under the self-schedule and price taker assumptions. While convenient, these assumptions neglect many aspects of the complex interactions between IES and markets.

2.3. Price taker optimization neglects how participants influence market outcomes

IES design, operation, and control decisions are inherently coupled and thus require simultaneous multiscale optimization [16, 25] while considering interactions with the electric grid, other energy infrastructures and supply chains, the economy, and the environment [9]. Recent examples of IES process synthesis and design optimization include biorefineries with power generation [31, 32]; water treatment with power generation [33]; heating, cooling, and power systems for residential complexes [34]; and processes to convert poultry litter to fertilizers, fuels, and power [35]. Many of these and similar studies use multi-objective optimization to analyze the trade-offs among competing goals such as economics, environmental impact, water usage, and energy consumption. Because of the diversity of technology options and the variety of timescales, it is challenging to cre-

ate a generalized modeling framework to quantify IES and grid interactions rigorously. Technology and timescale-specific assumptions and model reduction techniques are often applied to expedite a specific analysis. For instance, representative days are often used to optimize the design of variable renewables such as wind and solar. However, a different approach is needed to model the seasonal feedstock variability for a biomass IES. Many IES conceptual design studies use superstructure optimization [36, 37] to systematically select between technology alternatives while considering dynamic operations such as time-varying energy prices, dispatch signals, or energy and mass holdups. For example, Li and Zhang [38] proposed a basic IES structure containing an energy production system, an energy conversion system, and an energy storage system, as well as connections to the end user to optimize three objectives: annualized total cost, primary energy consumption, and carbon emissions. Demirhan et al. [39] proposed an alternative generalized IES superstructure encoding multiple chemical and fuel synthesis routes and power generation routes. They considered process design, operation, and supply chain management in their optimization strategy. The resulting MILP model incorporates hourly, daily, and seasonal fluctuations in renewable availability via a hierarchical clustering technique. Some studies also optimize subsystem capacities such as energy storage size [40, 41], equipment sizing and control decisions for polygeneration generators [42], and inputs and outputs for different configurations of a hybrid feedstock to liquids and electricity process [43]. Zhang et al. [44] optimize a process network for the production of fuels and power using solely renewable energy sources. The work considers both design decisions and scheduling based on time-varying renewable availability. Their results emphasize that for systems using time-varying resources (e.g., renewable energy sources), not considering operational decisions during the design phase can lead to sub-optimal process synthesis. Gabrielli and colleagues [45] proposed a novel MILP approach to optimize the selected technologies and operation schedule of a multi-energy system that allows an hourly resolution (refined enough to consider the operation of seasonal energy storage) while maintaining a small number of binary variables. Their approach produced results in good agreement with the full-scale optimization model and found that seasonal operation cycles can reduce CO₂ emissions. Kasivisvanathan et al. [46] used a robust MILP model to compute design decisions for multifunctional energy systems such as polygeneration generators and biorefineries with power production. Process units are black-box or scale-invariant models, which can be operated at a baseline state or adjusted to meet new demands/adjust for uncertainty in different predefined operating scenarios. Guo et al. [47] optimized the size and operation of a

regionally integrated energy system (RIES) while considering user-side demand response, modeled as an MINLP. The RIES model includes demand response for electric load, heat load, and cold load, inputs energy output and on/off status of technical equipment, demand response details (amount available, timing, economic compensation), and state variables including economic equipment technical parameters and energy demand. The model is optimized via a performance index that includes economic benefits of supply and user side, peak-to-valley ratios, and carbon emissions, and outputs optimal demand response schemes, installed capacity, and hourly energy output of technical equipment. The study found that implementing demand response increases energy efficiency and contributes to peak-shaving and valley-filling. In these studies, IES market interactions are modeled as time-varying prices or demands using the price taker and self-schedule assumptions, if at all.

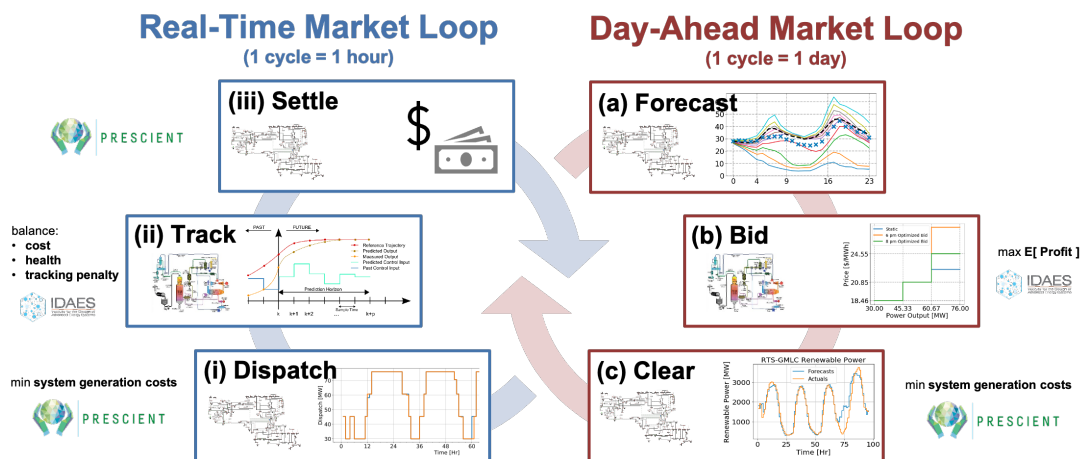


Figure 1: The multiscale optimization workflow from Gao et al. [16] captures complex interactions from IES and grid decision-making processes. In the day-ahead market loop, an IES uses market forecasts (a) to compute an optimal bidding strategy, (b) which constitutes a bid curve that reflects product costs. This information is input for *Prescient*, the production cost model, which (c) clears the market and sets the day-ahead dispatch schedule. In the real-time market loop, *Prescient* (i) updates the dispatch schedule, which is then communicated to all market participants. The IES then solves a (ii) tracking optimization problem to meet the requested dispatch while minimizing its costs and maximizing system health. Finally, *Prescient* (iii) calculates settlement payments.

A few recent studies have more explicitly modeled the complex interactions between IESs and the electric grid. Gao et al. [16] proposed a multiscale optimization framework, shown in Figure 1, that integrates optimized bidding, unit commitment (day-ahead market clearing), economic dispatch (real-time market clearing), model predictive control (MPC) to track market dispatch,

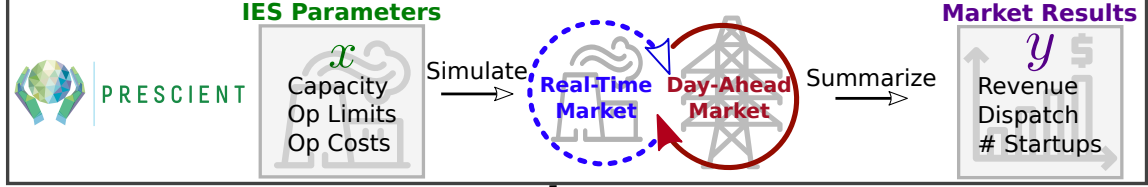
and market settlement calculations to simulate the performance of an IES interacting in an electric grid. Their results highlight the importance of detailed market simulations, demonstrating that a single IES optimal bidding into the market affects prices and dispatch signals throughout the network. They also show that hybridizing a thermal generator with energy storage reduces wear-and-tear (e.g., ramping, startups, mileage) for the thermal generators. As described above, the self-schedule and price taker assumptions are the current state-of-the-art, with a few exceptions. While optimal self-schedule performs better than heuristic scheduling, these methods can reduce revenue compared to submitting economic bids to a market operator [2]. A large body of prior work details the limits of generators choosing to self-schedule in this modern two-settlement system [48, 49, 50]. Orvis and Aggarwal (2018) [49] point out that operational flexibility already exists in the current system and that by removing the option for participants to self-schedule, the grid could operate more efficiently. Martinek et al. (2018) [50] compare self-scheduling (price taker) and system-scheduling (production cost modeling) solutions to optimize the dispatch of a concentrated solar power (CSP) plant in a regional system derived from the Western Electricity Coordinating Council’s (WECC) 2024 Common Case database [51]. Their results show that self-schedule methods over-estimate net annual revenue by up to 13% versus PCM due to price suppression caused by the CSP generator, and they suggest that the discrepancy may not warrant the computational effort required to perform large-scale PCM simulation studies for the purpose of design optimization. They caution, however, that small perturbations to their PCM dataset can drastically shift LMPs if such changes result in the dispatch of high-cost generators. Consequently, the authors conclude that PCM simulation should still be used to vet system design configurations obtained using price taker methods, especially under highly variable scenarios. A handful of studies evaluate the limitations of the price taker approach [52, 53, 54, 55, 56]. In general, these works demonstrate that price taker tends to overestimate the value of energy systems, especially for integrated systems and renewables, by not considering their impact on setting LMPs and their greater impact on price-setting in comparatively smaller ancillary service markets (the place where much of these systems’ revenue can be earned).

3. Methods

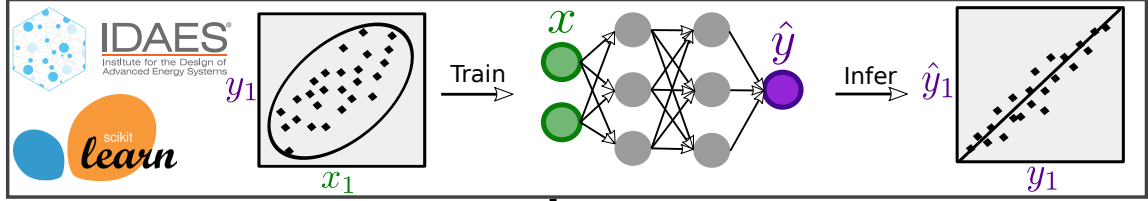
3.1. Problem Statement and Overview

Given a transmission network and electricity market, we seek to co-optimize the design and operation of an IES to replace a specified generator while explicitly considering IES market interactions.

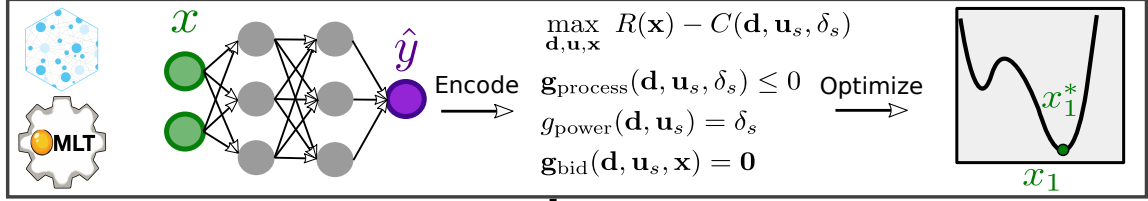
1. Run Market Simulations



2. Fit Market Surrogates



3. Optimize IES



4. Verify IES Design

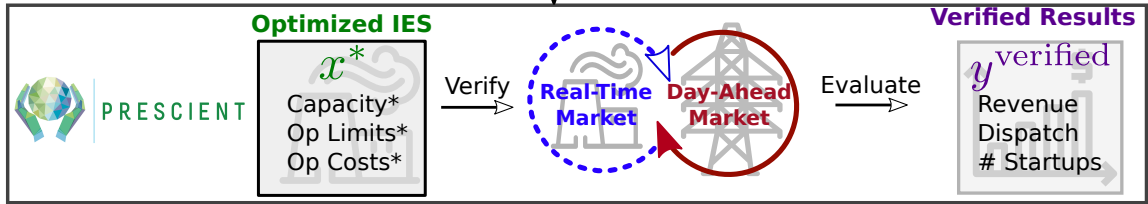


Figure 2: Summary of the proposed IES conceptual design workflow, including four main steps: (1) assemble the market simulation datasets, (2) train market surrogates, (3) optimize IES design using surrogates, and (4) verify candidate solutions with simulation.

Figure 2 shows the key steps of the proposed computational framework:

1. Run market simulations using a production cost model (PCM) to systematically characterize how varying generator attributes (e.g., P_{min} , P_{max} , and ramp-rate) changes market outcomes, including annual revenue, capacity factor, and startup events. (Section 3.2)
2. Using the simulation dataset from Step 1, train neural network (NN) and algebraic surrogates models to predict market outcomes as a function of IES design decisions and other market inputs. (Section 3.3)
3. Co-optimize IES design and operations decisions using the surrogate models from Step 2 to directly embed complex IES market interactions. Alternatively, the IES can be co-optimized using only time-varying price data from Step 1 using the price taker assumption, which serves as a benchmark for the proposed method. (Section 3.4)
4. Perform a PCM simulation for the optimal solution from Step 3 to verify the results and quantify the error in actual market outcomes as predicted by either the surrogates or price taker assumption. (Section 3.5)

Section 3.6 summarizes the energy system models used in the case study. Table 1 defines the nomenclature.

3.2. Step 1: Prescient Production Cost Model and RTS-GMLC Network

Without loss of generality, we design an energy system to replace a single coal-powered generator, named 123-STEAM-3, in the RTS-GMLC test system. For each replacement scenario, we systematically modify the design parameters of 123-STEAM-3, including P_{max} , ramp-rate, and marginal cost, and simulate the entire electricity market over a year to obtain economic outputs (e.g., revenue and capacity factor). We use RTS-GMLC, which is a publicly available, open-source test network that qualitatively mimics the Southwest United States power system [57, 58]. This study and many similar analyses in power systems engineering rely on test networks such as RTS-GMLC because real transmission network topology data is often protected. Other modern publicly-available test systems include the TAMU networks [59], ReEDS [60], and the high-resolution US test system [61]. Gao et al.[16] provides a comprehensive overview of the RTMS-GLMC test system.

We use PCM simulations to train surrogate models that learn electricity market outcomes. A PCM emulates the sequence of decisions made by grid operators to economically commit and dispatch generators within the bulk electric grid to meet total demand. The problems solved in PCM

Index and Set	Description
$s \in \mathcal{S} := \{1, \dots, N_s\}$	Price taker scenarios in Eq. (3)
$z \in \mathcal{Z} := \{z_{\text{off}}, z_1, \dots, z_{10}\}$	Dispatch zones, scenarios in Eq. (4)
Variable or Parameter	Description
N_B, β_j	Number of terms in basis function surrogate, coefficient for term j
W_k, \mathbf{b}_k	Neural network weights for layer k , neural network bias for layer k
\mathbf{x}	Inputs of market clearing, IES submits to market, see Table 2
$\mathbf{x}^L, \mathbf{x}^U$	Lower bounds on market inputs, upper bounds on market inputs
y_1, y_2, y_z	Outputs of market clearing, IES receives from market, see Table 2
\mathbf{d}	Plant design variables (e.g. $P_{max}, P_{min}, R_{rate}, UT, DT$)
$\mathbf{u}, \mathbf{u}_s, \mathbf{u}_z$	Plant operational variables, for scenario s , for zone z
w_s	Weight for scenario s
π_s	Price for scenario s , [$\frac{\$}{\text{MWh}}$]
$\delta, \delta_s, \delta_z$	Power output variables, for scenario s , for zone z , [MW]
\mathbf{y}_s	Binary variables indicating plant is on/off for scenario s
P_{max}, P_{min}	Maximum plant capacity, minimum plant output, [MW]
R_{rate}	Maximum plant ramp rate, [$\frac{\text{MW}}{\text{hr}}$]
UT, DT	Minimum plant up time, minimum plant down time, [hr]
$c_{P_{min}}^{op}, c_{P_{max}}^{op}$	Operating cost at P_{min} , operating cost at P_{max} , [$\frac{\$}{\text{hr}}$]
$c_{fixed}^{op}, c_{startup}^{op}$	Fixed operating cost [$\frac{\$}{\text{hr}}$], startup cost [$\$$]
ϵ^2	Small number (10^{-6})
Functions	Description
$\hat{y}^{alamo}(\cdot), f_j^{basis}(\cdot)$	ALAMO basis function surrogate, basis function term j
$\hat{\mathbf{y}}^{nn}(\cdot), \mathbf{f}_k(\cdot), \sigma(\cdot)$	Neural network surrogate, layer k function, layer activation function
$y_1^{surrogate}(\cdot), y_2^{surrogate}(\cdot), y_z^{surrogate}(\cdot)$	Surrogate functions to calculate: y_1, y_2 , and y_z
$R(\cdot), N(\cdot), w_z(\cdot)$	Functions to calculate: revenue, number of startups, weight for zone z
$C_{OPEX}(\cdot), C_{CAPEX}(\cdot), C_{startup}(\cdot)$	Functions to calculate: operating expense, capital expense, startup cost
$\mathbf{g}_{\text{process}}(\cdot)$	Plant process constraints (e.g. equipment constraints, control limits)
$g_{\text{power}}(\cdot)$	Plant power output constraint
$\mathbf{g}_{\text{bid}}(\cdot)$	Constraint that links plant variables with market variables

Table 1: Nomenclature

include load forecasting, unit commitment, unit dispatch, and calculation of financial settlements. PCM can be used to simulate both day-ahead and real-time markets and can consider transactions for both energy and ancillary services. PCM simulations determine how often a generator is dispatched and what electricity price it receives as payment.

For our study, we use the open-source **Prescient** [62] PCM to simulate the annual performance of our generator within the RTS-GMLC network. **Prescient** simulates real-time and day-ahead energy markets as depicted by the inner and outer cycles in Figure 1. The outer cycle solves a Unit-Commitment (UC) optimization problem, which schedules changes in the online status of each generator. In this cycle, **Prescient** forecasts non-dispatchable renewable generation and total load at each network bus, receives bids from generators and load-serving entities, and clears the market by committing generation to cover demand at the lowest possible cost. The inner, more frequent cycle solves a Security-Constrained-Economic-Dispatch (SCED) problem every hour to adjust the dispatch (output) for each committed generator from the previous UC problem. Generators track the demand signal from the dispatch and settle payments based on their delivery. **Prescient** has been used to simulate the operation of general wholesale electricity markets in the United States [63].

We perturb generator parameters for the energy system that replaces 123-STEAM-3 in the **Prescient** simulations as denoted in Table 2. These inputs (or values derived from them) are typical parameters communicated to ISOs for commitment and dispatch. The key design inputs include the maximum operating capacity x_1 (P_{max}), the minimum power output multiplier x_2 (which corresponds to the lower operating level P_{min}), the ramp-rate multiplier x_3 (which informs the true generator ramp-rate), the minimum uptime x_4 , and the downtime multiplier x_5 (downtime as a percentage of minimum up-time). These inputs are assumed fixed in day-to-day operation, reflecting the generator has been built. The more variable inputs include the marginal cost x_6 , the no-load cost x_7 , and a representative startup cost profile x_8 .

The marginal cost is communicated to ISOs as hourly step-wise bid curves of power-price pairs. These pairs represent the minimum price a generator needs to receive to dispatch the associated power output each hour. For our study, we use a single marginal cost representing the minimum price the generator must receive to operate at its minimum output or higher. The no-load cost is the cost of keeping a generator “spinning,” but not generating output. No-load cost is the fixed cost of operation that is independent of the amount of energy generated. For instance, a thermal generator’s no-load cost could be the cost to keep the turbine spinning at synchronous speed but not generating any output. The startup cost is the cost incurred to bring a generator online. A startup cost profile quantifies the incremental fuel costs associated with hot, warm, and cold starts.

Table 2 also lists the primary simulation outputs of interest, including the annual revenue y_1 ,

the total number of startup events y_2 , and the number of hours spent at each of 11 different power output zones y_z where $z \in \mathcal{Z} := \{z_{\text{off}}, z_1, \dots, z_{10}\}$. Zone z_{off} corresponds to a shutdown state, and the other ten zones represent intermediate generator output levels (i.e., z_1 is 0-10% output, and z_{10} is 90-100% output). A full factorial design over Table 2 results in 64,800 **Prescient** simulations requiring over 10,000 CPU days to complete. Each simulation is independent, however, which facilitates parallel execution. We performed our simulations on the Sandia SkyBridge cluster consisting of 1848 compute nodes each containing 16 cores (2.6 GHz Intel Sandy BridgeE5-2670 2S x 8C) and 64 GB of memory.

Input/Output	Description	Units	Simulation Levels	Base RTS-GMLC
x_1	Maximum Designed Capacity (P_{max})	MW	177, 266, 355, 443	350
x_2	Minimum Operating Multiplier	—	0, 0.15, 0.3, 0.45	0.4
x_3	Ramp Rate Multiplier	—	0.5, 0.75, 1.0	1.15
x_4	Minimum Up Time	hr	1, 2, 4, 8, 16	24
x_5	Minimum Down Multiplier	—	0.5, 1, 2	2
x_6	Marginal Cost	$\frac{\$}{\text{MWh}}$	5, 10, 15, 20, 25, 30	24.42
x_7	No Load Cost	$\frac{\$}{\text{MWh}}$	0, 1.0, 2.5	1.0
x_8	Startup Profile	—	0, 1, 2, 3, 4	2
y_1	Annual Revenue	\$MM	-	38.9
y_2	Annual Number of Startups	#	-	40
y_z	Annual Hours Dispatched in Zone z	hr	-	-

Table 2: Description of **Prescient** simulation input parameters and output variables. Data was adapted from RTS-GMLC[64].

The startup profile x_8 is a categorical variable described in Table 3. For our study, a startup cost profile value of 0 corresponds to a theoretical fast start unit with no startup cost, and each integer from 1 to 4 corresponds to a different thermal generator. The startup cost has units of $\frac{\$}{\text{MW}}$ and is the cost per capacity to bring the generator online. The lag ratio corresponds to the time required after a shutdown for a generator to enter a 'Warm' or 'Cold' state and is calculated as the required time to elapse as a ratio of the minimum downtime. For example, a large coal unit (profile 2) with a minimum downtime of 8 hours becomes 'Cold' if it is shut down for more than 16 hours. Our optimization formulations do not account for time-dependent startup costs, so we instead use the representative cost in Table 3 as an approximation in our optimization formulation in Section 3.4.2. Future work includes incorporating the lag ratios and multiple startup costs.

Startup Profile	Generator Type	Startup Costs $\frac{\$}{\text{MW}}$			Lag Ratio			Representative Cost $\frac{\$}{\text{MW}}$
		Hot	Warm	Cold	Hot	Warm	Cold	
0	Fast Start	0	0	0	-	-	1.0	0
1	NGCC Unit	35	50	79	-	-	1.0	79
2	Large Coal Unit	59	61	105	-	1.0	2.0	83
3	Medium Coal Unit	94	101	147	1.0	1.375	7.5	101
4	Small Coal Unit	94	135	147	1.0	2.5	3.0	135

Table 3: Description of generator startup profiles. NGCC means Natural Gas Combined Cycle. Data was adapted from RTS-GMLC[64].

3.3. Step 2: Surrogate Models for Market Outcomes

Our **Prescient** simulation dataset is used to train surrogate models that predict the outputs y_1 (annual revenue), y_2 (number of startups per year), and y_z (number of hours spent operating in each zone z per year) given the eight inputs in Table 2. Developing surrogate models is a broad field and covers many techniques such as response surfaces, kriging, Gaussian processes, neural networks, decision trees, and others [65]. We choose surrogate models that permit smooth general algebraic representations. Such surrogates can naturally be embedded within mathematical optimization frameworks and provide derivative information. Our surrogates include algebraic basis functions (which are linear combinations of nonlinear functions provided by Eq. (1)) and feed-forward neural networks (which are compositions of nonlinear transformations provided by Eq. (2)). There are advantages to developing both surrogates for our study. Algebraic basis functions are easier to interpret because the regressed coefficients explain which inputs are important and whether there are input interactions. Neural networks, on the other hand, can achieve great accuracy but are difficult to interpret.

To train algebraic basis functions, we use **ALAMO** [66] (version 2021.12.28) with the **IDAES-PSE** interface [67], which simplifies training and inference. **ALAMO** basis functions are described by Equation (1) where the output $\hat{y}^{\text{alamo}}(\mathbf{x})$ is evaluated given the input vector \mathbf{x} . Here f_j^{basis} represents basis function j , β_j is the coefficient for basis function j , and N_B is the number of considered basis functions.

$$\hat{y}^{\text{alamo}}(\mathbf{x}) = \sum_{j=1}^{N_B} \beta_j f_j^{\text{basis}}(\mathbf{x}) \quad (1)$$

We consider only monomial and binomial basis functions with power values of 1, 2, and 3, e.g., x_1^2 ,

$x_1 \cdot x_2$, and $(x_2 \cdot x_3)^3$, and we allow a maximum of 15 total terms ($N_B = 15$). We use Bayesian Information Criteria (BIC) implemented in ALAMO to choose the best algebraic surrogate using enumeration mode, i.e., ALAMO solves a series of ordinary least squares regression problems to select the basis functions. We train 13 surrogate models corresponding to each output: annual revenue y_1 , number of annual startups y_2 , and annual hours in each zone y_z in set \mathcal{Z} (explained above). Section S2 in the Supporting Information (SI) shows the obtained algebraic ALAMO surrogates.

We also train feed-forward neural networks (NNs) of the form given by Eq. (2) where we denote $\hat{\mathbf{y}}^{\text{nn}}$ as the NN output, which is evaluated given the input vector \mathbf{x} . Eq. (2a) expresses the NN as a composition of functions defined over K layers where $\mathbf{f}_k \circ \mathbf{f}_{k-1}$ means the output of function \mathbf{f}_{k-1} on layer $k-1$ is the input to layer k . Each layer function output $\mathbf{f}_k(\mathbf{z})$ is obtained according to Eq. (2b) by applying the activation function σ_k to the weighted sum of its inputs $W_k \mathbf{z}$ and the bias term \mathbf{b}_k . NNs can also be described structurally as directed acyclic graphs with nodes structured into K layers where each node applies the activation function to the weighted sum of its inputs. The structured representation is intuitive and easy to understand, but we elect the mathematical representation here to facilitate our design problem formulation. We finally note that a neural network produces a multivariate output unlike basis functions trained with ALAMO.

$$\hat{\mathbf{y}}^{\text{nn}}(\mathbf{x}) = \mathbf{f}_K \circ \mathbf{f}_{K-1} \circ \cdots \circ \mathbf{f}_2 \circ \mathbf{f}_1(\mathbf{x}) \quad (2a)$$

$$\mathbf{f}_k(\mathbf{z}) = \sigma_k(W_k \mathbf{z} + \mathbf{b}_k), \quad \forall k \in \{1, \dots, K\} \quad (2b)$$

For NN training, we use the MLPRegressor from scikit-learn version 0.23.1 with default settings to train three 2-layer neural networks: one NN surrogate to predict revenue (scalar), another NN to predict the number of startups (scalar), and a third NN to predict the time spent in each operating zone (vector). The revenue and startup surrogates contain 100 nodes in the first layer and 50 in the second. The zone surrogate comprises two layers of 100 nodes with 11 outputs (one for each zone). All nodes apply the hyperbolic tangent (tanh) activation function. We use the OMLT package[68] to formulate algebraic representations of each NN within our optimization model.

3.4. Step 3: Optimization Formulations for Steady-State Design and Operation

The goal of energy system co-optimization is to compute the best design decisions, represented by the vector \mathbf{d} , and operating decisions, represented by the vector \mathbf{u} , while considering interactions with electricity markets or other energy infrastructure captured by the market surrogates that map

generator characteristics \mathbf{x} to market outcomes \mathbf{y} . We now define two distinct co-optimization formulations considering steady-state IES process models.

3.4.1. Steady-State Co-Optimization with Price Taker and Self-Schedule

As discussed earlier, most studies in the literature invoke price taker and self-schedule assumptions to simplify the co-optimization problem. Under the price taker assumption, one assumes the energy system is sufficiently small to not impact the market operations and the resulting localized marginal prices (LMPs) for electricity. Likewise, in a self-schedule mode, the energy system does not submit a bid curve to the market. Instead, it decides the amount of electricity it will produce and is subject to the resulting market prices (it still submits a schedule to the ISO). While the key focus of this study is to develop market surrogates for co-optimization, it is helpful to compare these common assumptions. With price taker self-schedule, the design optimization problem input data are a pairwise series of price data and the corresponding frequency (weight), denoted by the pairs (π_s, w_s) contained in the set $s \in \mathcal{S} = \{1, \dots, N_s\}$. Given these data, the co-optimization problem is formulated as a two-stage stochastic program:

$$\max_{\mathbf{d}, \mathbf{u}, \delta} \sum_{s \in \mathcal{S}} w_s \left(R(\mathbf{d}, \mathbf{u}_s, \pi_s, \delta_s, \mathbf{y}_s) - C_{\text{OPEX}}(\mathbf{d}, \mathbf{u}_s, \delta_s, \mathbf{y}_s) \right) - C_{\text{CAPEX}}(\mathbf{d}) \quad (3a)$$

$$\text{s.t. } \mathbf{g}_{\text{process}}(\mathbf{d}, \mathbf{u}_s) \leq \mathbf{0}, \quad s \in \mathcal{S} \quad (3b)$$

$$g_{\text{power}}(\mathbf{d}, \mathbf{u}_s) = \delta_s, \quad s \in \mathcal{S} \quad (3c)$$

$$\mathbf{y}_s \in \{0, 1\}, \quad s \in \mathcal{S} \quad (3d)$$

In Eq. (3) the price and weight data π_s and w_s define the scenario set \mathcal{S} . The operating decisions, \mathbf{u}_s , and power output, δ_s , are indexed by scenario, thus making them *stage-two variables*. In contrast, the design decisions, \mathbf{d} , are identical across all scenarios and are *stage-one variables*. The objective function, Eq. (3a), computes revenue minus the operating costs as $R(\mathbf{d}, \mathbf{u}_s, \pi_s, \delta_s, \mathbf{y}_s) - C_{\text{OPEX}}(\mathbf{d}, \mathbf{u}_s, \delta_s, \mathbf{y}_s)$ for each scenario s and calculates the average revenue over the scenario set \mathcal{S} using the frequency weights w_s . Note that though the proposed formulation ignores temporal-based constraints, the formulation can still accommodate modeling if the plant is on or off through the binary variable \mathbf{y}_s for each scenario s . By including the on-off constraint, this resulting problem is a mixed-integer nonlinear programming problem (MINLP). The net profit is obtained by subtracting the capital cost $C_{\text{CAPEX}}(\mathbf{d})$. One of the simplest ways to define \mathcal{S} is by using historical time-series

price data where each time step is a distinct scenario and the weights are equal. Alternatively, as discussed in Section 4.3, histogram binning may be applied to generate more compact scenario sets. Within each scenario, Eq. (3b) models the IES equality or inequality constraints that relate the design and operating variables, \mathbf{d} and \mathbf{u}_s , respectively. Likewise, Eq. (3c) computes the power output δ_s as a (nonlinear) function of \mathbf{d} and \mathbf{u}_s for each scenario $s \in \mathcal{S}$.

3.4.2. Steady-State Co-Optimization with Market Interactions

While the price taker and self-schedule design problem, Eq. (3), is easy to implement and the de facto standard in literature (see references in Section 2), it has several disadvantages. Most importantly, Eq. (3) neglects two important aspects of how energy systems interact with wholesale electricity markets. First, the price taker assumption assumes prices will not be suppressed due to market participation. This can lead to erroneous revenue estimates if the additional generation shifts the market clearing price. Second, self-schedule is not viable for large generation units as they submit bid curves to manage price risk. Another challenge with Eq. (3) is that binary variables are required to model the on-off constraints, which scales the number of binary variables in the problem with a number of scenarios considered in \mathcal{S} . In this work, we propose a new co-optimization formulation, Eq. (4), that addresses these challenges:

$$\max_{\mathbf{d}, \mathbf{u}, \mathbf{x}} R(\mathbf{x}) - C_{\text{CAPEX}}(\mathbf{d}) - C_{\text{startup}}(\mathbf{d})N(\mathbf{x}) - \sum_{z \in \mathcal{Z}} w_z(\mathbf{x})C_{\text{OPEX}}(\mathbf{d}, \mathbf{u}_z, \delta_z) \quad (4a)$$

$$\text{s.t. } \mathbf{g}_{\text{process}}(\mathbf{d}, \mathbf{u}_z, \delta_z) \leq 0, \quad \forall z \in \mathcal{Z} \quad (4b)$$

$$g_{\text{power}}(\mathbf{d}, \mathbf{u}_z) = \delta_z, \quad \forall z \in \mathcal{Z} \quad (4c)$$

$$\mathbf{g}_{\text{bid}}(\mathbf{d}, \mathbf{u}_z, \mathbf{x}) = \mathbf{0}, \quad \forall z \in \mathcal{Z} \quad (4d)$$

$$w_z(\mathbf{x}) = \frac{\tilde{\text{m}}\text{ax}(y_z^{\text{surrogate}}(\mathbf{x}), 0)}{\sum_{j \in \mathcal{Z}} \tilde{\text{m}}\text{ax}(y_j^{\text{surrogate}}(\mathbf{x}), 0)}, \quad (\text{Zone Surrogates}) \quad \forall z \in \mathcal{Z} \quad (4e)$$

$$R(\mathbf{x}) = \tilde{\text{m}}\text{ax}(y_1^{\text{surrogate}}(\mathbf{x}), 0), \quad (\text{Revenue Surrogate}) \quad (4f)$$

$$N(\mathbf{x}) = \tilde{\text{m}}\text{ax}(y_2^{\text{surrogate}}(\mathbf{x}), 0), \quad (\text{Startup Surrogate}) \quad (4g)$$

$$\max(a, 0) \approx \tilde{\text{m}}\text{ax}(a, 0) = \frac{1}{2} \left(a + \sqrt{a^2 + \epsilon^2} \right). \quad (\text{Smoothed Max}) \quad (4h)$$

Eq. (4) is also a two-stage stochastic program with the set of zones \mathcal{Z} as scenarios. The design decisions, \mathbf{d} , and bid parameters, \mathbf{x} , are the *stage-one variables*. Likewise, the operating decisions,

\mathbf{u}_s , are the *stage-two variables*. In the objective function, Eq. (4a), the net profit is calculated as the market revenue minus the costs (CAPEX, OPEX, and startup). Here the market revenue, $R(\mathbf{x})$, is a function of the bid parameters, \mathbf{x} , outlined in Table 2. The function $R(\mathbf{x})$ is connected to the surrogates (discussed in Section 3.3) via Eq. (4f). The function $C_{\text{startup}}(\mathbf{d})$ calculates startup cost as a function of the design variables, and Eq. (4g) is the annual number of startups predicted by $y_2^{\text{surrogate}}(\mathbf{x})$. This surrogate formulation incorporates startup cost in a steady-state model without temporal constraints. In contrast, Eq. (3) cannot incorporate startup cost without including temporal constraints, which would make it a multi-period (and not steady-state) model. The remaining costs $C_{\text{OPEX}}(\mathbf{d}, \mathbf{u}_z, \delta_z)$ are averaged over the scenarios $z \in \mathcal{Z}$. Recall that in the price taker self-schedule formulation, Eq. (3), the weights for all scenarios w_s were input data. In contrast, for this formulation, the frequency of each scenario, $w_z(\mathbf{x})$, is the time-quantity of interest for capturing operating costs, e.g., the fraction of hours operating at each power output, and depends on the bid parameters. Eq. (4e) connects $w_z(\mathbf{x})$ to the zone dispatch surrogates described in Section 3.3. The functions $R(\mathbf{x})$, $N(\mathbf{x})$, and $w_z(\mathbf{x})$ use a smoothed max operator to eliminate negative predictions, which can arise from inaccuracies of the surrogates in specific regions of the design space, where ϵ^2 in Eq. (4h) is a small number (we use $\epsilon^2 = 10^{-6}$). Analogous to Eq. (3), Eqs. (4b) and (4c) contain the IES process models and relate the design \mathbf{d} and operating \mathbf{u}_z variables to the power output δ_z for each scenario $z \in \mathcal{Z}$. Similarly, Eq. (4d) links the process variables \mathbf{d} and \mathbf{u}_z to the bid (market) variables \mathbf{x} . Thus for Eq. (4), the input data are the power output δ_z for each scenario and the market surrogates $y_1^{\text{surrogate}}(\mathbf{x})$, $y_2^{\text{surrogate}}(\mathbf{x})$, and $y_z^{\text{surrogate}}(\mathbf{x})$. This new co-optimization formulation replaces the price taker and self-schedule assumptions central to Eq. (3) with surrogate models, which incorporate how participating in the market directly impacts the revenue and dispatch for the energy system (generator).

Eqns. (4b) and (4c) are direct analogs to Eqns. (3b) and (3c) as they describe the same physical constraints. Eq. (4b) represents physical generator limits, and Eq. (4c) requires power output to track the demand signal for each zone/scenario.

Eq. (5) gives the bid parameters used in this study, which contain the 8 bid parameters from Table 2. Here, (5a) denotes limits on \mathbf{x} where \mathbf{x}^L and \mathbf{x}^U are lower and upper bounds, respectively, for each bid variable. Eq. (5b) connects x_1 to the generator design capacity P^{max} , (5c) links x_2 to the minimum operating capacity P^{min} , (5d) links x_3 to the ramp rate R^{rate} , (5e) links x_4 to the minimum up time UT , and (5f) links x_5 to the minimum down time DT . Next, Eq. (5g) connects

the average generator operating cost to the marginal cost bid variable x_6 . We denote the operating cost at P_{min} as $c_{P_{min}}^{op}$ and at P_{max} as $c_{P_{max}}^{op}$. Eq. (5h) links fixed costs c_{fixed}^{op} to the no-load cost bid variable x_7 and Eq. (5i) links the startup cost $c_{startup}^{op}$ to the bid variable x_8 .

$$\mathbf{x}^L \leq \mathbf{x} \leq \mathbf{x}^U \quad \text{Bid Limits} \quad (5a)$$

$$x_1 = P_{max} \quad \text{Maximum Capacity} \quad (5b)$$

$$x_2 \cdot P_{max} = P_{min} \quad \text{Minimum Capacity} \quad (5c)$$

$$x_3(P_{max} - P_{min}) = R_{rate} \quad \text{Ramp Rate} \quad (5d)$$

$$x_4 = UT \quad \text{Minimum Up Time} \quad (5e)$$

$$x_5 \cdot UT = DT \quad \text{Minimum Down Time} \quad (5f)$$

$$x_6 = \frac{1}{2} \left(\frac{c_{P_{min}}^{op}}{P_{min}} + \frac{c_{P_{max}}^{op}}{P_{max}} \right) \quad \text{Marginal Cost} \quad (5g)$$

$$x_7 \cdot P_{max} = c_{fixed}^{op} \quad \text{No-Load Cost} \quad (5h)$$

$$x_8 \cdot P_{max} = c_{startup}^{op} \quad \text{Startup Cost} \quad (5i)$$

Note that some bid variables describe time-dependent quantities. Particularly, the terms for ramp rate and up/downtime are dynamic attributes linked to the bid variables x_3 , x_4 , and x_5 . The steady-state formulation described by Eq. (4) does not physically capture these time-dependent variables. Still, the bid parameters themselves can be used to approximate what the market outcomes would be. Also, recall that x_8 is a representative cost corresponding to a discrete startup profile. This variable can be treated in Eq. (4) as a degree of freedom using integer optimization, but we choose to fix it for this study to a nominal value (although it would be easy to enumerate the five different values). We note that more detailed bid formulations use a marginal cost curve instead of the average operating cost described by Eq. (5g). A marginal cost curve is important for sophisticated bidding strategies like those performed in [16].

3.5. Step 4: Verification

Solving either Eq. (3) or (4) produces a design candidate we can verify with additional market simulations. The obtained optimal bid parameters, \mathbf{x} , become inputs to a PCM (e.g., **Prescient**), which simulates the actual unit states (on/off), LMPs, and dispatch of each market participant. The number of startups for our candidate generator is obtained from the unit state, and the revenue is calculated using the simulated dispatch and LMPs. The verified operating cost requires fixing

the power output in the IES process model to the dispatch signal and calculating the cost for each hour. We use nominal values for the ramp rates, up/down times, and startup costs to verify the price taker formulation.

3.6. Case Study: Energy System Model

This case study uses the Rankine cycle illustrated and described in Figure 3 as the representative supercritical thermal steam generator. The mathematical model is developed in the IDAES-PSE computational platform and includes mass and energy balances and thermodynamic properties for water and steam calculated using the IAPWS-95 property package. A single steady-state instance of the square model (when the inlet boiler feed water flowrate is fixed) contains 59 variables and 59 equations. Figure S5 in the Supporting Information shows the capital cost as a function of the maximum power capacity. Similarly, Figure S6 shows operating cost, heat rate, and cycle efficiency as a function of operating capacity. The DISPATCHES (Design Integration and Synthesis Platform to Advance Tightly Coupled Hybrid Energy Systems) project GitHub repository¹ contains a full description of the implemented model and code. Using the simple model, we demonstrate the proposed framework and meaningfully contrast the results with those obtained from the benchmark self-schedule price taker formulation. We emphasize that the proposed framework is general purpose and that this energy system model is an illustrative case study.

¹<https://github.com/gmlc-dispatches/dispatches>

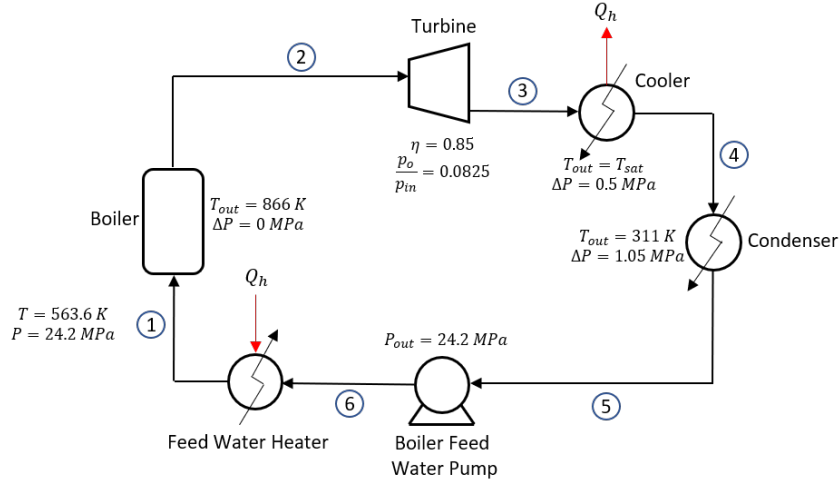


Figure 3: Simplified model for the supercritical steam generator energy system. The temperature and pressure of the inlet boiler feed water, stream ①, is set to 563.6 K and 24.2 MPa. The boiler is modeled using a heater with no pressure drop, and its outlet temperature, stream ②, is fixed to 866 K, which is the typical turbine inlet temperature for supercritical pulverized coal power plants. The turbine is modeled as an isentropic turbine with a pressure ratio of 0.082 and isentropic efficiency of 0.85. The outlet from the turbine, stream ③, is cooled in the cooler, with a pressure drop of 0.5 MPa, to a saturated liquid, stream ④. The heat recovered, Q_h , is transferred to the feed water heater, represented by the red arrow. The outlet temperature and pressure of the condenser, stream ⑤, is fixed to 311 K and 1.05 MPa respectively. The boiler feed water pump has a fixed efficiency of 0.8, and the outlet pressure is fixed to 24.2 MPa, stream ⑥. The outlet of the feed water heater, stream ①, is the inlet of the boiler.

4. Results

We now demonstrate the conceptual framework illustrated in Figure 2 to co-optimize the operation and design of an energy system while explicitly considering market interactions.

4.1. Sensitivity Analysis of Energy Market Simulations

To establish an intuition about the market, we search for trends across marginal costs, no-load costs, different startup profiles, and maximum design capacities while fixing other variables to nominal values. Table 4 defines the eight cases, and Figure 4 shows the simulation results for the annual revenue, the number of startups, and the capacity factor. Our two key observations from the eight cases are:

Revenue and capacity factor are sensitive to every studied bid parameter. Generator revenue almost always increases with higher P_{max} , which is expected; larger generators can deliver

more electricity and collect more revenue. Revenue is always higher for lower marginal cost cases (cases 1 through 4), which also confirms our intuition. The ISO dispatches the lowest-cost generators first, which leads to high capacity factors and more revenue. At high marginal costs (cases 5 through 8), both no-load and startup costs matter. The startup cost appears more important than the no-load cost as Case 6 outperforms Case 7. Case 8 rarely turns the generator on due to high marginal, no-load, and startup costs. Capacity factor shows the same trends as revenue, except it tends to decrease with high P_{max} values suggesting the additional output is not always used.

Generator startups are highly sensitive to the startup cost for any marginal cost.

All fast-start cost scenarios perform many startups throughout the year for low and high marginal cost cases. For high startup costs, the number of startups is always minimal, and the generator is either never dispatched or is never shut down. The no-load cost contributes to some variation in the number of startups.

We lastly highlight that a full global sensitivity analysis of our **Prescient** dataset was performed and is provided in Section S1 in the Supporting Information. The analysis further quantifies the effect of each individual market parameter on generator revenue and number of startups and is consistent with our observed trends.

Case	Marginal Cost $\frac{\$}{\text{MWh}}$	No Load Cost $\frac{\$}{\text{MWh}}$	Startup Profile (Generator Type)
1	15.0	0.0	0 (Fast Start Unit)
2	15.0	2.5	0 (Fast Start Unit)
3	15.0	0.0	4 (Small Coal Unit)
4	15.0	2.5	4 (Small Coal Unit)
5	25.0	0.0	0 (Fast Start Unit)
6	25.0	2.5	0 (Fast Start Unit)
7	25.0	0.0	4 (Small Coal Unit)
8	25.0	2.5	4 (Small Coal Unit)

Table 4: Eight scenarios for the parameterized energy system are defined for further analysis. Nominal values for each case are $x_2=0.3$, $x_3=1.0$, $x_4=4$, and $x_5=1$. Data were adapted from RTS-GMLC[64].

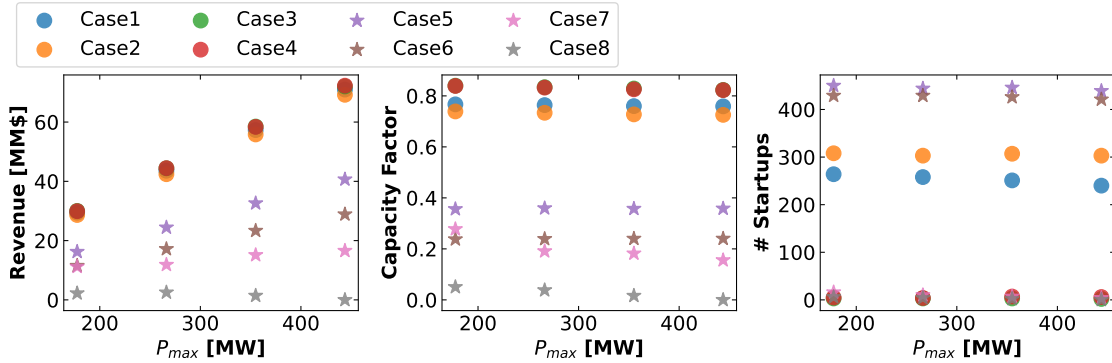


Figure 4: Prescient Sweep Summary. Cases correspond to Table 4. Dots are low marginal cost cases, and stars are high marginal cost cases.

4.2. Neural networks outperform algebraic surrogates

We train basis function (with ALAMO) surrogates and NN surrogates (with sci-kit learn) to predict the total revenue (y_1) and the number of startups (y_2) as a function of generator bid parameters (\mathbf{x}). Figure 5 shows the parity plots obtained using our test data for the ALAMO (top) and NN (bottom) surrogates for the revenue (y_1) and the number of startups (y_2). The obtained ALAMO R^2 values are 0.825 and 0.419 for the revenue and the number of startups, respectively, whereas the NN R^2 values are both greater than 0.99. The parity plots for the 11 zone surrogates support this conclusion and are available in the SI; Figure S2 shows all 11 ALAMO surrogate fits, and Figure S3 shows the zone NN surrogate fits.

Basis functions could not achieve accuracy comparable to the NNs for any of the

fitting options we tried in ALAMO. For instance, we saw no improvement in considering nonlinear basis functions or increasing the number of basis terms. The basis function surrogates do, however, provide a natural interpretation of their parameters through regression coefficients. For instance, the revenue basis function surrogate is dominated by coefficients for P_{max} and marginal cost terms, while other coefficients are close to zero. These coefficient fits are consistent with our sensitivity analysis. The basis function surrogates obtained with ALAMO are available in Section S2 in the Supporting Information.

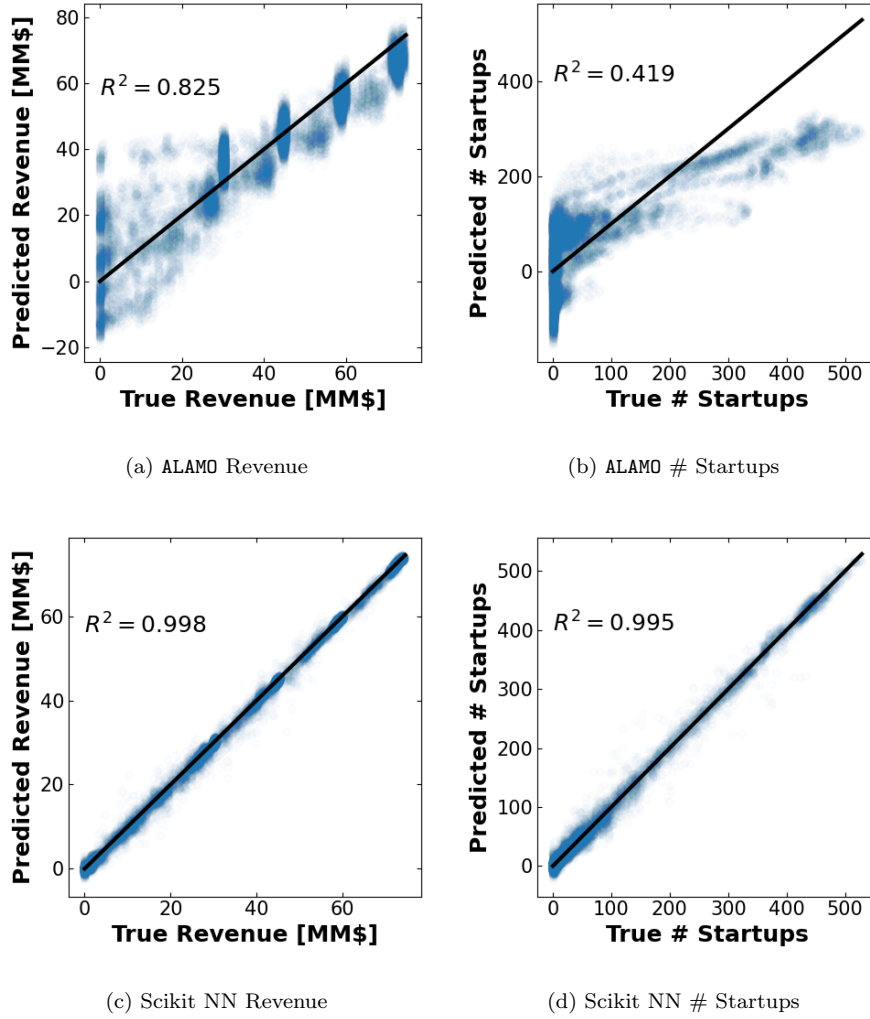


Figure 5: Parity Plots for Surrogate Models over Test Set Data. ALAMO revenue surrogate (top left), ALAMO startup surrogate (top right),

4.3. Steady-state conceptual design optimization with market surrogates is computationally tractable

Optimization with market-based surrogates, Eq. (4), is computationally efficient and provides verifiable candidate design solutions. Furthermore, our surrogates capture important dynamic effects that the price taker approach, Eq. (3), inherently cannot consider. Table 6 compares the two formulations for different fuel price and surrogate settings, which we discuss here. Specific

details of each problem formulation are described in the table caption. The surrogate predictions for capacity factor and operating cost correspond to the zone surrogates depicted in Figure 6. The intermediate zones provide small contributions to these predictions and can be found in Figure S4 in the Supporting Information. We now highlight six key observations from the results.

Conceptual design with market surrogates is computationally tractable. We use `Ipopt` [69] to solve each design problem with the `ma27` linear solver library [70]. The market surrogates produce moderately small optimization problems (order of hundreds of variables and constraints) that can be solved in seconds. In contrast, the price taker formulation size depends on the number of scenarios in \mathcal{S} . For example, the full-year price signal contains 8760 (hourly) scenarios, producing an optimization problem with more than 400,000 constraints and variables (after relaxing each binary \mathbf{y}_s to a continuous variable). Though the solution time to solve the rMINLP (NLP) with `Ipopt` is less than 100 seconds on average, the time required to build the model is around 2000 seconds. The price taker problem tractability can be improved by binning LMP scenarios in the set \mathcal{S} . Table 5 shows the optimal price taker solution for increasing numbers of binned LMPs where 100 bins are consistent with the full price signal solution, PT-1, in Table 6. For the market surrogate optimization formulation, we found it difficult to converge using basis function surrogates likely due to a small feasible space resulting from poor surrogate accuracy. Each NN surrogate, on the other hand, is solved in under a minute without requiring specialized initialization. While not the focus of this manuscript, incorporating predictive surrogates such as deep NNs into the optimization is a promising avenue for development.

No. of bins	Optimal P_{max} [MW]	Operating Cost [\$MM/yr]	Revenue [\$MM/yr]	Capacity Factor [-]	Startups [# /yr]
10	177.5	16.10	29.94	0.77	1
25	177.5	19.78	30.26	0.72	1
50	177.5	19.78	30.30	0.71	2
75	177.5	19.78	30.52	0.71	3
100	177.5	19.78	30.55	0.71	3
250	177.5	19.78	30.58	0.70	4
500	177.5	19.78	30.57	0.70	4

Table 5: Results from price taker using a binning approach to identify the price signals set.

Market surrogate accuracy translates to verified performance illustrated by comparing the NN-1 and ALAMO-1 results. NN-1 predicts the revenue and the operating cost with good accu-

racy, whereas ALAMO-1 demonstrates considerable error (see Figure 6). Coincidentally, ALAMO-1 almost predicts the verified 20-year net revenue because it falsely anticipates many startup events (and resulting costs) throughout the year. We highlight that, as expected, the surrogates predict a continuous number of starts.

The price taker assumption can perform well at low marginal costs. This intuitively makes sense; low marginal costs validate the price taker premise that the generator self-schedule is always dispatched. This is observed in Table 6 where PT-1 produces nearly the same generator as NN-1. Even at this low marginal cost, however, the price taker assumption over-predicts revenue and under-predicts operating cost, which leads to more than a \$10M disparity over 20 years.

Market surrogates capture dynamics that price taker representations cannot. PT-2 predicts a small capacity factor of 0.36 (0.33 verified) due to the expensive fuel price, i.e., the generator assumes it is only committed when the market prices are sufficiently high. However, the price taker formulation does not account for startups, and the verified startup costs are significant: \$16M over 20 years. PT-2 also over-predicts annual revenue, implying that price suppression may occur due to its participation. In contrast, NN-2 predicts a smaller capacity factor of 0.23 (0.25 verified), likely by accounting for startup costs and price suppression, i.e., the surrogate predicts that generator dispatch is shifted to higher prices.

Although NN-2 accurately predicts the capacity factor, we found that it over-predicts revenue and slightly under-predicts operating cost, which leads to notable verification errors. This discrepancy can be reduced via adaptive sampling or more sophisticated neural network architectures or both, which are left as future work. Interestingly, NN-2 builds almost the same generator as PT-2; the one key difference is the ramp rate. Section 4.4 further explores such design parameter effects.

Optimizing the bid marginal cost can affect generator dispatch. The NN-3 setting is equivalent to NN-1, but it decouples the marginal cost bid from the operating cost. Thus the cost curve in NN-3 does not reflect the true generator costs and can be adjusted to procure additional dispatch (lower marginal cost generators are dispatched first) or shift prices upwards (by making a higher-cost generator marginal). NN-3 predicts a slightly higher capacity factor and annual revenue versus NN-1 (which is verified by simulation) but produces lower net revenue because it is a local solution (NN-3 has more degrees of freedom than NN-1). While the virtual marginal cost bid leads to a similar market outcome in this setting, it incentivizes the exploration of advanced bidding strategies for hybrid systems with flexible marginal costs.

Optimization always builds the smallest generator possible because prices are too low. The most obvious result from Table 6 is that net revenue is always negative because annual revenue does not surpass the capital and operating costs. In hindsight, this makes sense; RTS-GMLC presents challenging economics for a conventional thermal generation exacerbated by using a copper plate assumption (neglecting transmission congestion). Future work includes exploring scenarios that lead to competitive economics such as using a less-overbuilt system, considering transmission constraints, or participating in ancillary service markets.

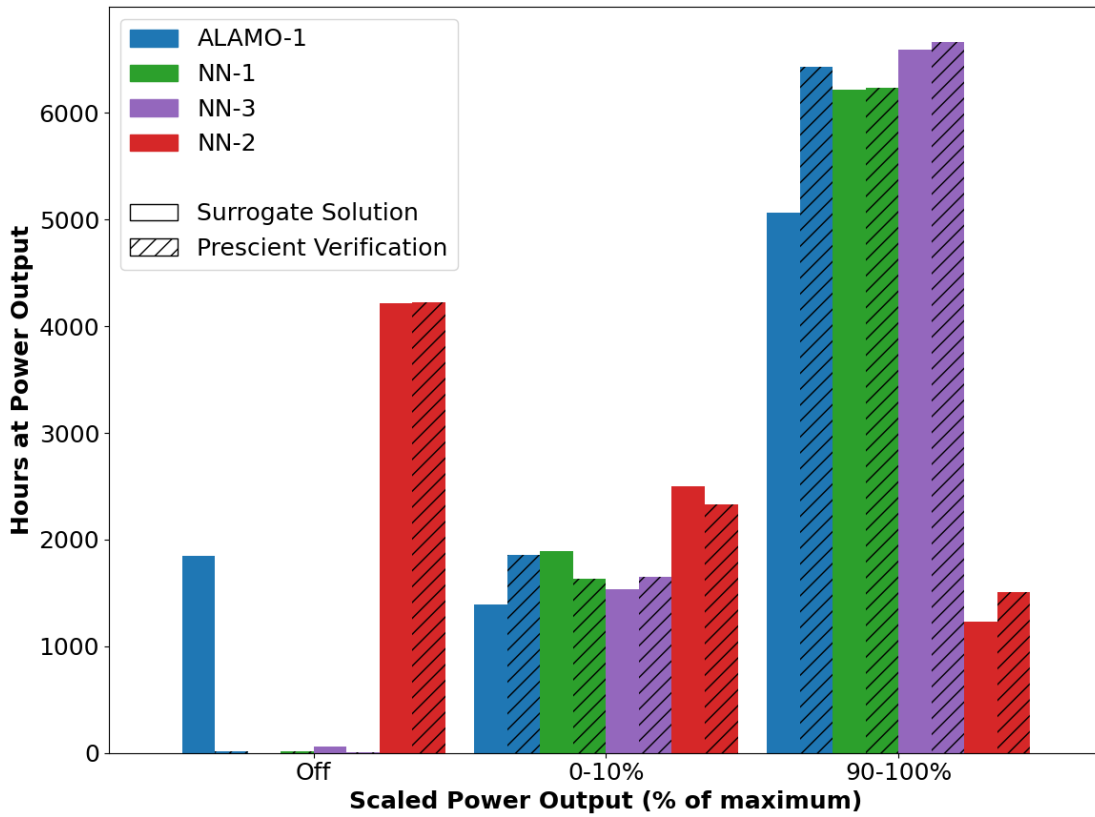


Figure 6: Verification of Market Interaction Solutions for Select Zone Surrogate Outputs. The bars depict the annual number of hours spent shutdown (off), operating at minimum capacity (0-10%), and operating at maximum capacity (90-100%) for ALAMO-1 (blue), NN-1 (green), NN-2 (red), and NN-3 (purple). Textured bars correspond to values verified by simulating in *Prescient*.

	PT-1	ALAMO-1	NN-1	PT-2	NN-2	NN-3
Fuel Price [\$/ton]	30.0	30.0	30.0	50.0	50.0	30.0
Marginal Cost Setting	-	Average	Average	-	Average	Free
Design Problem Solution						
Solution Time [s]	35	112*	22	89	29	50
Capital Cost [\$MM]	408	408	408	408	408	408
Pmax [MW]	177.5	177.5	177.5	177.5	177.5	177.5
Pmin-Multiplier[-]	0.15	0.15	0.176	0.15	0.15	0.15
Ramp-Multiplier[-]	-	1.0	0.86	-	0.63	0.9
Marginal Cost[\$/MWh]	17.54	17.54	17.49	25.76	25.76	13.25
Design Problem Outputs						
Capacity Factor [-]	0.79	0.64	0.79	0.36	0.23	0.81
Startups [# /yr]	≤389	74.5	0.75	≤559	74.6	1.07
Operating Cost [\$MM/yr]	19.8	16.0	20.2	13.1	9.0	20.8
Startup Cost [\$MM/yr]	≤4.2	0.81	0.01	≤6.06	0.81	0.01
Revenue [\$MM/yr]	30.55	26.60	29.25	16.57	14.29	30.08
20 Year Net Revenue [\$MM]	-201.0	-212.8	-209.4	-339.2	-319.0	-222.4
Prescient Verified Outputs						
Capacity Factor [-]	0.80	0.79	0.80	0.33	0.25	0.82
Startups [# /yr]	2	3	3	74	66	1
Operating Cost [\$MM/yr]	20.3	20.2	20.4	12.6	9.7	20.8
Startup Cost [\$MM/yr]	0.02	0.03	0.03	0.80	0.72	0.01
Revenue [\$MM/yr]	30.15	29.87	30.13	15.36	12.30	30.46
20 Year Net Revenue [\$MM]	-212.3	-216.5	-214.4	-370.4	-371.2	-215.9

Table 6: Comparison of price taker and surrogate design solutions. PT-1 and PT-2 correspond to solving the price taker problem with cheap and expensive fuel, respectively. ALAMO-1 and NN-1 solve the surrogate design problem with cheap fuel using basis function and neural network surrogates. NN-2 solves the surrogate problem with a neural network for expensive fuel. NN-3 is the same as NN-1, but the marginal cost is a free variable. We use nominal values for the surrogate cases where we set $x_4=4.0$, $x_5 = 1.0$, $x_7 = 1.0$, and $x_8 = 2$. For both price taker problems, the number of hours off provides a conservative upper bound for the maximum possible number of startups (and their associated costs). *Problem required additional initialization to converge.

4.4. Surrogates emulate market interactions and go beyond price taker

The proposed surrogate framework captures dynamic market interactions, which can lead to more informed energy system design candidates. Consequently, we demonstrate *why* market dynamics should be captured in generator design and when it is important to go beyond the price taker and self-schedule assumptions. We expect market surrogates to perform reliably in various designs and operating conditions, whereas static price taker assumptions should fail when dynamics are important. With this motivation, we dive deeper into our simulation results and present three key findings.

The marginal cost of a single generator shifts LMPs. Figure 7 shows how the LMP distributions vary as a result of changing the marginal cost of generator 123-STEAM-3. Furthermore, we found that other design parameters had little effect on prices, which is shown by the lack of sensitivity to the startup profile (although other parameters do affect generator dispatch). Prices are suppressed when 123-STEAM-3 bids a very low marginal cost. We hypothesize the low-cost generator is scheduled, leading to lower market clearing prices. The average LMP notably increases when the marginal cost of 123-STEAM-3 exceeds 20.0 \$/MWh. This likely means that the generator becomes a marginal generator around this price. Considering our RTS-GMLC assumptions (e.g., copper plate), we expect more pronounced LMP variability in a more realistic power grid and plan to explore this in future work.

Price taker breaks down under realistic design scenarios as illustrated by Figure 8. The assumption works well for small generators with low marginal costs, as implied in Figure 8a. However, it over-predicts revenue for larger generators, likely due to not capturing price suppression. Moreover, the startup profile becomes a key design parameter at high marginal costs for which the steady-state price taker formulation cannot incorporate start-up costs. Interestingly, the plotted price taker solutions tend to track startup profile 0 (the fast-start unit), which implies the assumption can work for generator designs with very low startup costs. Moreover, the price taker formulation is an MINLP. In this case study, solving the relaxed MINLP finds 0 or 1 values for the relaxed binary variable. In contrast, the market surrogates formulation uses only continuous variables and circumvents the need for binary variables.

Marginal cost of a single generator perturbs marginal cost distribution in the grid. Figure S7 in the SI shows the capacity factors of generators in the grid, sorted from lowest to highest capacity factor in the nominal RTS-GMLC simulation, for P_{max} of 177.5 MW and 433.5

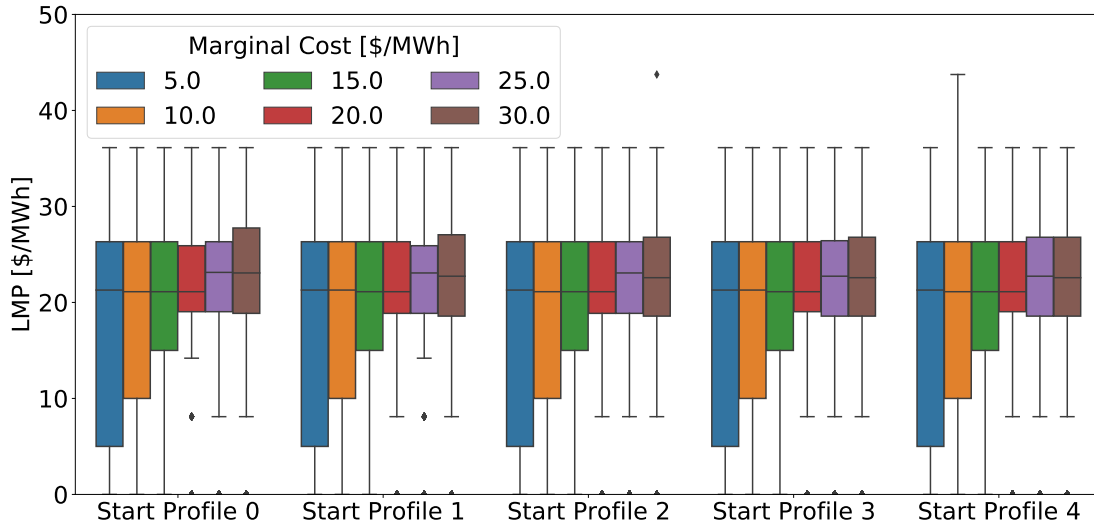
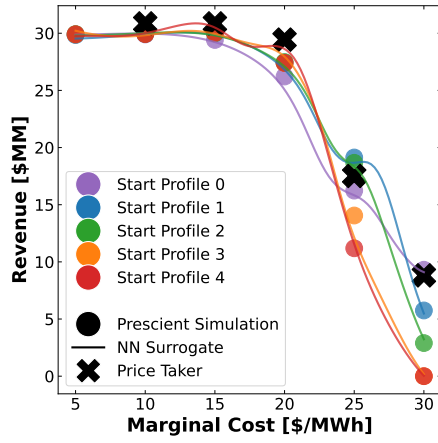


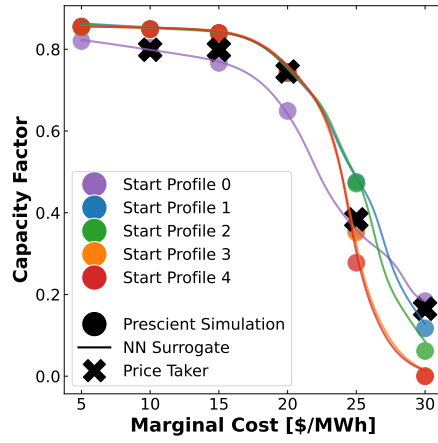
Figure 7: Summarized LMP distributions obtained from *Prescient* simulations. LMPs are grouped by the marginal cost and startup profile of generator 123-STEAM-3. All results correspond to a $P_{max}=433$ MW.

MW and marginal costs of 20-30 \$/MWh for the perturbed generator. Figure S8 further explores P_{max} of 433 MW P_{max} and 25 \$/MWh marginal cost. These figures show that at higher marginal costs (> 20 \$/MWh), running the perturbed generator at higher startup profiles causes other steam generators in the system to reduce their total dispatch leading to lower capacity factors, whereas low-dispatching generators in the system (especially combined cycle generators) dispatch more and attain higher capacity factors.

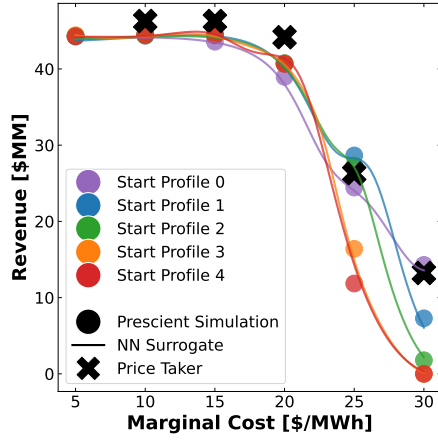
Optimization with market surrogates is accurate over a wide range of conditions. The surrogate predictions are verified by *Prescient* at low and high marginal costs for every startup profile. While very promising, we believe our market surrogates could be further improved. Table 6 shows that small revenue residuals lead to large errors in estimates over a 20-year time horizon. We are currently investigating adaptive sampling approaches to iteratively update surrogates as well as different NN architectures in future work.



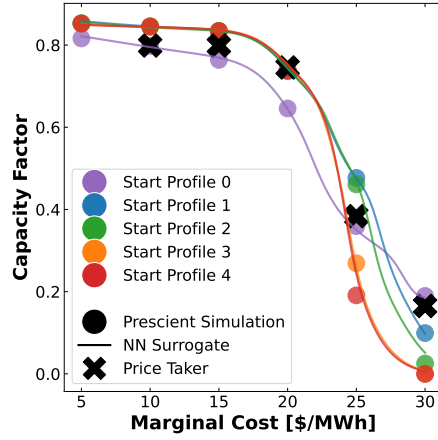
(a) Revenue ($P_{max}=177.5$)



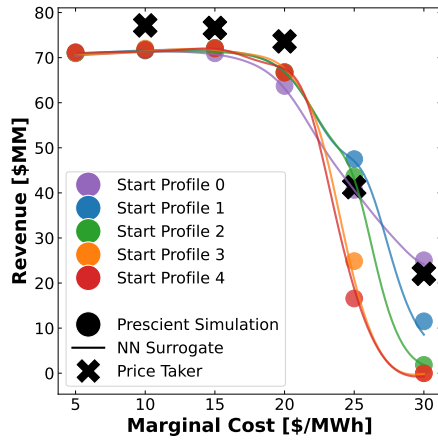
(b) Capacity Factor ($P_{max}=177.5$)



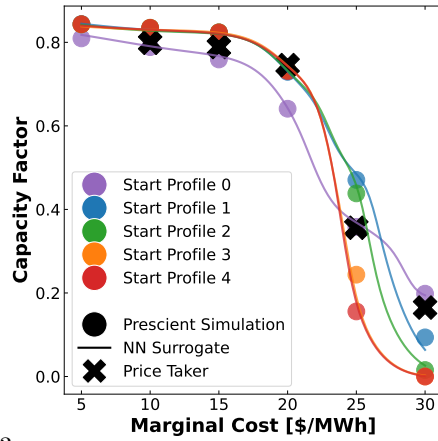
(c) Revenue ($P_{max}=266.75$)



(d) Capacity Factor ($P_{max}=266.75$)



(e) Revenue ($P_{max}=433.5$)



(f) Capacity Factor ($P_{max}=433.5$)

Figure 8: Comparison of surrogate and price taker predictions for revenue (left plots) and capacity factor (right plots) for different values of P_{max} , marginal cost, and startup profiles. Circles represent actual **Prescient** simulations, lines correspond to surrogate model evaluations, and cross symbols (\times) represent price taker solutions. The results were generated with $x_2=0.3$, $x_3=1.0$, $x_4=4$, $x_5=1$, and $x_7=0.0$ held constant.

5. Conclusions

IESs must be optimized in the context of the electric grid as represented by electricity markets to provide the necessary dynamic flexibility to support deep decarbonization through the adoption of non-dispatchable VREs. The current state-of-the-art approach is to co-optimize the design and operation of IESs using a two-stage stochastic program constructed with historical or forecasted data and the self-schedule and price taker assumptions. This paper proposes an alternative approach that uses machine learning and algebraic (basis function) surrogate models to embed IES market interactions directly into the co-optimization problem. We assemble a library of over 64,000 annual grid simulations, each corresponding to a different scenario of replacing one generator with a new candidate IES design. Global sensitivity analyses reveal that all eight generator characteristics communicated to the market, especially the nameplate capacity and marginal cost, influence the market outcomes (e.g., IES revenue, IES dispatch). We successfully train basis function and neural network surrogate models to predict these market outcomes as a function of the generator characteristics. We find the NN surrogate models vastly outperform basis functions for this large dataset. The highly accurate NN surrogates facilitate global sensitivity analysis, revealing the IES characteristics with the greatest impact on market outcomes. Using a thermal generator illustrative case study, we directly compare two co-optimization problem formulations: the de facto standard with price taker and self-schedule assumptions and our new formulation with market surrogates. Using annual market simulations to verify the results, we explain why the price taker and self-schedule assumptions break down at specific market conditions, such as high marginal costs. Thus, the key contribution of this work is demonstrating the limitations of the self-schedule and price taker assumptions and proposing a computationally tractable alternative capable of directly incorporating complex IES market interactions into multiscale optimization formulations. We emphasize the computational framework uses open-source software tools including the Pyomo modeling environment in Python, the IDAES (Institute for the Design of Advanced Energy Systems) Integrated Platform, the DISPATCHES (Design Integration and Synthesis Platform to Advance Tightly Coupled Hybrid Energy Systems) modeling library, the OMLT package, the **Prescient** production cost model (PCM), and the RTS-GMLC test network and associated data.

This paper presents a new multiscale optimization approach and simulation verification workflow, incentivizing several future search directions. Most notably, this paper focuses on steady-state co-optimization formulations. Extension to a multiperiod formulation that explicitly incorporates

time (essential to include energy storage or VREs properly) is left as future work. Multiperiod analysis requires a more sophisticated surrogate modeling strategy. We hypothesize this future enhancement will show that the self-schedule and price taker assumptions break down more dramatically for IES with energy storage and other subsystems that provide extensive dynamic flexibility. Similarly, we expect that using more sophisticated settings in the production cost model, such as transmission congestion or renewable uncertainty, will greatly diminish the accuracy of the price taker assumption and provide a greater incentive for using the proposed approach. We also anticipate the proposed framework can be applied with an order of magnitude fewer annual simulations in the training dataset, especially using adaptive sampling techniques. Another interesting possibility is building approximations for the PCM from historical data when the full network information is unavailable [71]. Finally, we reiterate that the proposed workflow uses open-source software tools, which creates almost endless opportunities to co-optimize different IES technologies in specific market contexts. As the electricity grid becomes more dynamic and integrated through the continuing growth of renewables, energy storage, and hydrogen, the methods described in this paper will be essential for evaluating and designing future energy generation technologies that most effectively contribute to regional energy infrastructures.

Acknowledgments

This work was conducted as part of the Design Integration and Synthesis Platform to Advance Tightly Coupled Hybrid Energy Systems (DISPATCHES) project through the Grid Modernization Lab Consortium with funding from the U.S. Department of Energy’s Office of Fossil Energy and Carbon Management, Office of Nuclear Energy, and Hydrogen and Fuel Cell Technology Office. Additional work was conducted as part of the Institute for the Design of Advanced Energy Systems (IDAES) with support through the Simulation-Based Engineering, Crosscutting Research Program within the U.S. Department of Energy’s Office of Fossil Energy and Carbon Management. Additional work was conducted in part by appointments for A.W.D. and X.G. to the U.S. Department of Energy (DOE) Postgraduate and Faculty Research Programs at the National Energy Technology Laboratory administered by the Oak Ridge Institute for Science and Education (ORISE).

This work was authored in part by authors at the National Renewable Energy Laboratory, operated by Alliance for Sustainable Energy, LLC, for the U.S. Department of Energy (DOE) under Contract No. DE-AC36-08GO28308, and authors at Lawrence Berkeley National Laboratory under

Contract No. DE-AC02-05CH11231 with the U.S. Department of Energy. Sandia National Laboratories is a multimission laboratory managed and operated by National Technology and Engineering Solutions of Sandia, LLC, a wholly owned subsidiary of Honeywell International, Inc., for the U.S. Department of Energy's National Nuclear Security Administration under contract DE-NA-0003525. This paper describes objective technical results and analysis. Any subjective views or opinions that might be expressed in the paper do not necessarily represent the views of the U.S. Department of Energy or the United States Government.

This paper was prepared as an account of work sponsored by an agency of the United States Government. Neither the United States Government nor any agency thereof, nor any of their employees, makes any warranty, express or implied, or assumes any legal liability or responsibility for the accuracy, completeness, or usefulness of any information, apparatus, product, or process disclosed, or represents that its use would not infringe privately owned rights. Reference herein to any specific commercial product, process, or service by trade name, trademark, manufacturer, or otherwise does not necessarily constitute or imply its endorsement, recommendation, or favoring by the United States Government or any agency thereof. The views and opinions of authors expressed herein do not necessarily state or reflect those of the United States Government or any agency thereof.

The U.S. Government retains and the publisher, by accepting the article for publication, acknowledges that the U.S. Government retains a nonexclusive, paid-up, irrevocable, worldwide license to publish or reproduce the published form of this work, or allow others to do so, for U.S. Government purposes.

Conflict of interest statement

Nothing to declare.

CRedit statement

J.J. Conceptualization, Methodology, Software, Formal Analysis, Investigation, Data Curation, Writing – Original Draft, Writing – Review & Editing, Visualization

J.G. Conceptualization, Methodology, Software, Formal Analysis, Investigation, Data Curation, Writing – Original Draft, Writing – Review & Editing, Visualization, Project Administration

N.C. Writing – Original Draft (literature review), Writing – Review & Editing
X.G. Methodology, Software, Data Curation, Writing – Review & Editing
B.K. Methodology, Software, Data Curation, Investigation, Writing – Review & Editing
D.A. Formal Analysis, Writing – Review & Editing, Visualization
S.M. Software, Writing – Review & Editing
X.C. Software
D.G. (NREL) Software
R.G.T. Software
L.B. Software
K.B. Software
D.G. (LBL) Software, Project Administration
J.D.S. Methodology, Project Administration
D.C.M. Project Administration, Funding Acquisition, Writing – Review & Editing
A.W.D. Conceptualization, Methodology, Software, Investigation, Data Curation, Writing –
Original Draft, Writing – Review & Editing, Visualization, Project Administration, Supervision

References

- [1] International Energy Agency, Global Energy & CO₂ Status Report 2019 – Analysis, Tech. rep. (2019).
- [2] E. Ela, M. Milligan, A. Bloom, A. Botterud, A. Townsend, T. Levin, Evolution of wholesale electricity market design with increasing levels of renewable generation, Tech. rep., National Renewable Energy Lab.(NREL) (2014).
- [3] L. Bird, D. Lew, M. Milligan, E. M. Carlini, A. Estanqueiro, D. Flynn, E. Gomez-Lazaro, H. Holttinen, N. Menemenlis, A. Orths, P. B. Eriksen, J. C. Smith, L. Soder, P. Sorensen, A. Altiparmakis, Y. Yasuda, J. Miller, Wind and solar energy curtailment: A review of international experience, *Renewable and Sustainable Energy Reviews* 65 (2016) 577–586. doi:10.1016/J.RSER.2016.06.082.
- [4] K. Imran, I. Kockar, A technical comparison of wholesale electricity markets in north america and europe, *Electric Power Systems Research* 108 (2014) 59–67. doi:10.1016/j.epsr.2013.10.016.

- [5] S. Bresler, The value of markets (2018).
URL <https://insidelines.pjm.com/the-value-of-markets/>
- [6] M. Alizadeh, M. P. Moghaddam, N. Amjady, P. Siano, M. Sheikh-El-Eslami, Flexibility in future power systems with high renewable penetration: A review, *Renewable and Sustainable Energy Reviews* 57 (2016) 1186–1193. doi:10.1016/j.rser.2015.12.200.
- [7] What the duck curve tells us about managing a green grid, Tech. rep., California Independent System Operator (CAISO) (2016).
- [8] P. LeMar, Integrated Energy Systems (IES) for Buildings: A Market Assessment, Tech. rep., Oak Ridge National Lab. (ORNL) (October 2002).
- [9] D. J. Arent, S. M. Bragg-Sitton, D. C. Miller, T. J. Tarka, J. A. Engel-Cox, R. D. Boardman, P. C. Balash, M. F. Ruth, J. Cox, D. J. Garfield, Multi-input, Multi-output Hybrid Energy Systems, *Joule* 5 (1) (2021) 47–58. doi:10.1016/j.joule.2020.11.004.
- [10] P. D. Lund, J. Lindgren, J. Mikkola, J. Salpakari, Review of energy system flexibility measures to enable high levels of variable renewable electricity, *Renewable and Sustainable Energy Reviews* 45 (2015) 785–807. doi:10.1016/J.RSER.2015.01.057.
- [11] Y. Sawle, S. C. Gupta, A. K. Bohre, Review of hybrid renewable energy systems with comparative analysis of off-grid hybrid system, *Renewable and Sustainable Energy Reviews* 81 (2018) 2217–2235. doi:10.1016/J.RSER.2017.06.033.
- [12] H. Wang, A. Saint-Pierre, P. Mancarella, System level cost and environmental performance of integrated energy systems: An assessment of low-carbon scenarios for the UK, 2015 IEEE Eindhoven PowerTech, *PowerTech 2015* (2015). doi:10.1109/PTC.2015.7232659.
- [13] M. S. Zantye, A. Arora, M. M. Faruque Hasan, Operational power plant scheduling with flexible carbon capture: A multistage stochastic optimization approach, *Computers and Chemical Engineering* 130 (2019) 106544. doi:10.1016/j.compchemeng.2019.106544.
- [14] A. Weidlich, D. Veit, A critical survey of agent-based wholesale electricity market models, *Energy Economics* 30 (4) (2008) 1728–1759. doi:10.1016/j.eneco.2008.01.003.

- [15] A. W. Dowling, R. Kumar, V. M. Zavala, A multi-scale optimization framework for electricity market participation, *Applied Energy* 190 (2017) 147–164. doi:10.1016/j.apenergy.2016.12.081.
- [16] X. Gao, B. Knueven, J. D. Sirola, D. C. Miller, A. W. Dowling, Multiscale simulation of integrated energy system and electricity market interactions, *Applied Energy* 316 (2022) 119017. doi:10.1016/j.apenergy.2022.119017.
- [17] P. Siano, Demand response and smart grids—a survey, *Renewable and sustainable energy reviews* 30 (2014) 461–478.
- [18] A. W. Dowling, T. Zheng, V. M. Zavala, Economic assessment of concentrated solar power technologies: A review, *Renewable and Sustainable Energy Reviews* 72 (2017) 1019–1032. doi:10.1016/j.rser.2017.01.006.
- [19] R. Walawalkar, J. Apt, R. Mancini, Economics of electric energy storage for energy arbitrage and regulation in new york, *Energy Policy* 35 (4) (2007) 2558–2568. doi:10.1016/j.enpol.2006.09.005.
- [20] F. Jabari, B. Mohammadi-ivatloo, M. Mohammadpourfard, Robust optimal self-scheduling of potable water and power producers under uncertain electricity prices, *Applied Thermal Engineering* 162 (2019) 114258. doi:10.1016/J.APPLTHERMALENG.2019.114258.
- [21] A. Attarha, N. Amjady, S. Dehghan, B. Vatani, Adaptive Robust Self-Scheduling for a Wind Producer with Compressed Air Energy Storage, *IEEE Transactions on Sustainable Energy* 9 (4) (2018) 1659–1671. doi:10.1109/TSTE.2018.2806444.
- [22] A. Bischi, L. Taccari, E. Martelli, E. Amaldi, G. Manzolini, P. Silva, S. Campanari, E. Macchi, A rolling-horizon optimization algorithm for the long term operational scheduling of cogeneration systems, *Energy* 184 (2019) 73–90. doi:10.1016/J.ENERGY.2017.12.022.
- [23] R. L. Fares, M. E. Webber, A flexible model for economic operational management of grid battery energy storage, *Energy* 78 (2014) 768–776. doi:10.1016/j.energy.2014.10.072.
- [24] R. L. Fares, J. P. Meyers, M. E. Webber, A dynamic model-based estimate of the value of a vanadium redox flow battery for frequency regulation in texas, *Applied Energy* 113 (2014) 189–198.

- [25] F. Sorourifar, V. M. Zavala, A. W. Dowling, Integrated multiscale design, market participation, and replacement strategies for battery energy storage systems, *IEEE Transactions on Sustainable Energy* 11 (1) (2018) 84–92. doi:10.1109/TSTE.2018.2884317.
- [26] C. T. Elmore, A. W. Dowling, Learning spatiotemporal dynamics in wholesale energy markets with dynamic mode decomposition, *Energy* 232 (2021) 121013. doi:10.1016/j.energy.2021.121013.
- [27] A. W. Dowling, T. Zheng, V. M. Zavala, A decomposition algorithm for simultaneous scheduling and control of csp systems, *AIChE Journal* 64 (7) (2018) 2408–2417. doi:10.1002/aic.16101.
- [28] A. W. Dowling, V. M. Zavala, Economic opportunities for industrial systems from frequency regulation markets, *Computers & Chemical Engineering* 114 (2018) 254–264. doi:10.1016/j.compchemeng.2017.09.018.
- [29] A. W. Dowling, B. L. Nicholson, Uncovering new opportunities from frequency regulation markets with dynamic optimization and pyomo.dae, in: *Computer Aided Chemical Engineering*, Vol. 44, Elsevier, 2018, pp. 2509–2514. doi:10.1016/B978-0-444-64241-7.50413-4.
- [30] J. Eichman, A. Townsend, M. Melaina, Economic assessment of hydrogen technologies participating in california electricity markets, Tech. rep., National Renewable Energy Lab.(NREL) (2016).
- [31] B. Wang, B. H. Gebreslassie, F. You, Sustainable design and synthesis of hydrocarbon biorefinery via gasification pathway: Integrated life cycle assessment and technoeconomic analysis with multiobjective superstructure optimization, *Computers & Chemical Engineering* 52 (2013) 55–76. doi:10.1016/J.COMPCHEMENG.2012.12.008.
- [32] S. Y. Tey, S. S. Wong, J. A. Lam, N. Q. Ong, D. C. Foo, D. K. Ng, Extended hierarchical decomposition approach for the synthesis of biorefinery processes, *Chemical Engineering Research and Design* 166 (2021) 40–54. doi:10.1016/J.CHERD.2020.11.015.
- [33] S. F. Mussati, M. Barttfeld, P. A. Aguirre, N. J. Scenna, A disjunctive programming model for superstructure optimization of power and desalting plants, *Desalination* 222 (1-3) (2008) 457–465. doi:10.1016/J.DESAL.2007.01.162.

- [34] L. F. Fuentes-Cortés, A. W. Dowling, C. Rubio-Maya, V. M. Zavala, J. M. Ponce-Ortega, Integrated design and control of multigeneration systems for building complexes, *Energy* 116 (2016) 1403–1416. doi:10.1016/j.energy.2016.05.093.
- [35] J. Ma, F. You, Superstructure optimization of thermal conversion based poultry litter valorization process, *Journal of Cleaner Production* 228 (2019) 1111–1121. doi:10.1016/J.JCLEPRO.2019.04.346.
- [36] J. Gong, F. You, Sustainable design and synthesis of energy systems, *Current Opinion in Chemical Engineering* 10 (2015) 77–86. doi:10.1016/j.coche.2015.09.001.
- [37] L. Mencarelli, Q. Chen, A. Pagot, I. E. Grossmann, A review on superstructure optimization approaches in process system engineering, *Computers & Chemical Engineering* 136 (2020) 106808. doi:10.1016/j.compchemeng.2020.106808.
- [38] Y. Li, R. Zhang, Study on the operation strategy for integrated energy system with multiple complementary energy based on developed superstructure model, *International Journal of Energy Research* 43 (13) (2019) 6951–6969. doi:10.1002/ER.4712.
- [39] C. D. Demirhan, W. W. Tso, J. B. Powell, E. N. Pistikopoulos, A multi-scale energy systems engineering approach towards integrated multi-product network optimization, *Applied Energy* 281 (2021) 116020. doi:10.1016/J.APENERGY.2020.116020.
- [40] G. Wang, A. Mitsos, W. Marquardt, Conceptual design of ammonia-based energy storage system: System design and time-invariant performance, *AIChE Journal* 63 (5) (2017) 1620–1637. doi:10.1002/AIC.15660.
- [41] H. Li, C. Zhang, B. Sun, Optimal design for component capacity of integrated energy system based on the active dispatch mode of multiple energy storages, *Energy* 227 (2021) 120522. doi:10.1016/J.ENERGY.2021.120522.
- [42] Y. Chen, X. Li, T. A. Adams, P. I. Barton, Decomposition strategy for the global optimization of flexible energy polygeneration systems, *AIChE Journal* 58 (10) (2012) 3080–3095. doi:10.1002/AIC.13708.

- [43] C. He, F. You, X. Feng, A novel hybrid feedstock to liquids and electricity process: Process modeling and exergoeconomic life cycle optimization, *AICHE Journal* 60 (11) (2014) 3739–3753. doi:10.1002/AIC.14551.
- [44] Q. Zhang, M. Martín, I. E. Grossmann, Integrated design and operation of renewables-based fuels and power production networks, *Computers & Chemical Engineering* 122 (2019) 80–92. doi:10.1016/J.COMPHEMENG.2018.06.018.
- [45] P. Gabrielli, M. Gazzani, E. Martelli, M. Mazzotti, Optimal design of multi-energy systems with seasonal storage, *Applied Energy* 219 (2018) 408–424. doi:10.1016/J.APENERGY.2017.07.142.
- [46] H. Kasivisvanathan, A. T. Ubando, D. K. Ng, R. R. Tan, Robust optimization for process synthesis and design of multifunctional energy systems with uncertainties, *Industrial & Engineering Chemistry Research* 53 (8) (2014) 3196–3209. doi:10.1021/ie401824j.
- [47] Z. Guo, R. Zhang, L. Wang, S. Zeng, Y. Li, Optimal operation of regional integrated energy system considering demand response, *Applied Thermal Engineering* 191 (2021) 116860. doi:10.1016/J.APPLTHERMALENG.2021.116860.
- [48] J. Kazempour, B. F. Hobbs, Value of flexible resources, virtual bidding, and self-scheduling in two-settlement electricity markets with wind generation—part i: principles and competitive model, *IEEE Transactions on Power Systems* 33 (1) (2017) 749–759. doi:10.1109/TPWRS.2017.2699687.
- [49] R. Orvis, S. Aggarwal, Refining competitive electricity market rules to unlock flexibility, *The Electricity Journal* 31 (5) (2018) 31–37. doi:10.1016/j.tej.2018.05.012.
- [50] J. Martinek, J. Jorgenson, M. Mehos, P. Denholm, A comparison of price-taker and production cost models for determining system value, revenue, and scheduling of concentrating solar power plants, *Applied Energy* 231 (2018) 854–865. doi:10.1016/j.apenergy.2018.09.136.
- [51] Teppc study report – 2024 pc1 common case and release notes for wecc 2024 common case version 1.1, Tech. rep., Western Electricity Coordinating Council (WECC) (2015).

- [52] B. Frew, D. Levie, J. Richards, J. Desai, M. Ruth, Analysis of multi-output hybrid energy systems interacting with the grid: Application of improved price-taker and price-maker approaches to nuclear-hydrogen systems, *Applied Energy* 329 (2023) 120184. doi:10.1016/j.apenergy.2022.120184.
- [53] H. Ding, P. Pinson, Z. Hu, J. Wang, Y. Song, Optimal offering and operating strategy for a large wind-storage system as a price maker, *IEEE Transactions on Power Systems* 32 (6) (2017) 4904–4913. doi:10.1109/TPWRS.2017.2681720.
- [54] M. I. Emmanuel, P. Denholm, A market feedback framework for improved estimates of the arbitrage value of energy storage using price-taker models, *Applied Energy* 310 (2022) 118250. doi:10.1016/j.apenergy.2021.118250.
- [55] J. Arteaga, H. Zareipour, A price-maker/price-taker model for the operation of battery storage systems in electricity markets, *IEEE Transactions on Smart Grid* 10 (6) (2019) 6912–6920. doi:10.1109/TSG.2019.2913818.
- [56] J. A. Sousa, F. Teixeira, S. Faias, Impact of a price-maker pumped storage hydro unit on the integration of wind energy in power systems, *Energy* 69 (2014) 3–11. doi:10.1016/j.energy.2014.03.039.
- [57] C. Grigg, P. Wong, P. Albrecht, R. Allan, M. Bhavaraju, R. Billinton, Q. Chen, C. Fong, S. Haddad, S. Kuruganty, W. Li, R. Mukerji, D. Patton, N. Rau, D. Reppen, A. Schneider, M. Shahidehpour, C. Singh, The ieeereliability test system-1996. a report prepared by the reliability test system task force of the application of probability methods subcommittee, *IEEE Transactions on Power Systems* 14 (3) (1999) 1010–1020. doi:10.1109/59.780914.
- [58] C. Barrows, A. Bloom, A. Ehlen, J. Ikäheimo, J. Jorgenson, D. Krishnamurthy, J. Lau, B. McBennett, M. O’Connell, E. Preston, et al., The ieeereliability test system: A proposed 2019 update, *IEEE Transactions on Power Systems* 35 (1) (2019) 119–127. doi:10.1109/TPWRS.2019.2925557.
- [59] H. Li, J. L. Wert, A. B. Birchfield, T. J. Overbye, T. G. S. Roman, C. M. Domingo, F. E. P. Marcos, P. D. Martinez, T. Elgindy, B. Palmintier, Building highly detailed synthetic electric grid data sets for combined transmission and distribution systems, *IEEE Open Access Journal of Power and Energy* 7 (2020) 478–488. doi:10.1109/OAJPE.2020.3029278.

- [60] S. M. Cohen, J. Becker, D. A. Bielen, M. Brown, W. J. Cole, K. P. Eurek, A. Frazier, B. A. Frew, P. J. Gagnon, J. L. Ho, P. Jadun, T. T. Mai, M. Mowers, C. Murphy, A. Reimers, J. Richards, N. Ryan, E. Spyrou, D. C. Steinberg, Y. Sun, N. M. Vincent, M. Zwerling, Regional energy deployment system (reeds) model documentation: Version 2018, Tech. rep., National Renewable Energy Lab. (NREL) (April 2019).
- [61] Y. Xu, N. P. Myhrvold, D. Sivam, K. Mueller, D. J. Olsen, B. Xia, D. Livengood, V. Hunt, B. R. d’Orfeuil, D. B. C. Muldrew, M. Ondreicka, M. Bettilyon, U.s. test system with high spatial and temporal resolution for renewable integration studies, 2020 IEEE Power & Energy Society General Meeting (PESGM) (2020) 1–5.
- [62] J. P. Watson, B. Knueven, R. Concepcion, D. Melander, A. Short, P. Zhang, D. Woodruff, Prescient, [Computer Software] <https://doi.org/10.11578/dc.20201101.1> (May 2020). doi:10.11578/dc.20201101.1.
- [63] B. Knueven, J. Ostrowski, J.-P. Watson, On mixed-integer programming formulations for the unit commitment problem, *INFORMS Journal on Computing* 32 (4) (2020) 857–876. doi:10.1287/ijoc.2019.0944.
- [64] Reliability Test System Grid Modernization Lab Consortium (RTS-GMLC) data repository (2022).
URL <https://github.com/GridMod/RTS-GMLC>
- [65] A. Bhosekar, M. Ierapetritou, Advances in surrogate based modeling, feasibility analysis, and optimization: A review, *Computers & Chemical Engineering* 108 (2018) 250–267. doi:<https://doi.org/10.1016/j.compchemeng.2017.09.017>.
URL <https://www.sciencedirect.com/science/article/pii/S0098135417303228>
- [66] A. Cozad, N. V. Sahinidis, D. C. Miller, Learning surrogate models for simulation-based optimization, *AIChE Journal* 60 (6) (2014) 2211–2227. doi:10.1002/aic.14418.
- [67] A. Lee, J. H. Ghouse, J. C. Eslick, C. D. Laird, J. D. Siirola, M. A. Zamarripa, D. Gunter, J. H. Shinn, A. W. Dowling, D. Bhattacharyya, L. T. Biegler, A. P. Burgard, D. C. Miller, The idaes process modeling framework and model library—flexibility for process simulation and optimization, *Journal of Advanced Manufacturing and Processing* 3 (3) e10095. doi:10.1002/amp2.10095.

- [68] F. Ceccon, J. Jalving, J. Haddad, A. Thebelt, C. Tsay, C. D. Laird, R. Misener, Omlt: Optimization & machine learning toolkit, *Journal of Machine Learning Research* 23 (349) (2022) 1–8.
- [69] A. Wächter, L. T. Biegler, On the implementation of an interior-point filter line-search algorithm for large-scale nonlinear programming, *Mathematical Programming* 106 (1) (2006) 25–57.
- [70] HSL, A collection of fortran codes for large scale scientific computation.
URL <http://www.hsl.rl.ac.uk/>
- [71] N. Cortes, X. Gao, B. Knueven, A. W. Dowling, Estimating energy market schedules using historical price data, in: *Computer Aided Chemical Engineering*, Vol. 49, Elsevier, 2022, pp. 517–522.
- [72] A. Saltelli, M. Ratto, T. Andres, F. Campolongo, J. Cariboni, D. Gatelli, M. Saisana, S. Tarantola, *Global sensitivity analysis: the primer*, John Wiley & Sons, 2008.
- [73] B. Iooss, P. Lemaître, A review on global sensitivity analysis methods, *Uncertainty Management in Simulation-Optimization of Complex Systems* (2015) 101–122doi:10.1007/978-1-4899-7547-8_5.
- [74] I. M. Sobol, Global sensitivity indices for nonlinear mathematical models and their monte carlo estimates, *Mathematics and Computers in Simulation* 55 (1-3) (2001) 271–280. doi:10.1016/S0378-4754(00)00270-6.
- [75] K. Seongho, *ppcor*: An R package for a fast calculation to semi-partial correlation coefficients, *Communications for Statistical Applications and Methods* 22 (6) (2015) 665–674. doi:10.5351/CSAM.2015.22.6.665.
- [76] J. Whittaker, *Graphical models in applied multivariate statistics*, Wiley Publishing, 2009.
- [77] J. Herman, W. Usher, SALib: An open-source Python library for sensitivity analysis, *Journal of Open Source Software* 2 (9) (2017) 97. doi:10.21105/joss.00097.

Supporting Information: Beyond Price Taker: Conceptual Design and Optimization of Integrated Energy Systems using Machine Learning Market Surrogates

Jordan Jalving^{1,5}, Jaffer Ghouse², Nicole Cortes³, Xian Gao³, Bernard Knueven⁴, Damian Agi³, Shawn Martin¹, Xinhe Chen³, Darice Guittet⁴, Radhakrishna Tumbalam-Gooty², Ludovico Bianchi⁶, Keith Beattie⁶, Daniel Gunter⁶, John D. Sirola¹, David C. Miller², and Alexander W. Dowling^{3,1}

¹*Sandia National Laboratories, Albuquerque, NM 87123*

²*National Energy Technology Laboratory, Pittsburgh, PA 15236*

³*Department of Chemical and Biomolecular Engineering,
University of Notre Dame, Notre Dame, IN 46556*

⁴*National Renewable Energy Technology Laboratory, Golden, CO 80401*

⁵*Pasteur Labs, Brooklyn, NY 11205*

⁶*Lawrence Berkeley National Laboratory, Berkeley CA 94720*

S1. Sensitivity Analysis

We apply well-known correlation and variance-based global sensitivity analysis (GSA) methods [72, 73] to our **Prescient** simulation dataset to *quantify* the importance of each market parameter with respect to revenue, dispatch, and number of generator startups. We calculate different correlation coefficients given by Eq. (S1) and Eq. (S2), and different Sobol sensitivity measures denoted by Eq. (S3) for each input/output pair in Table 2. We expect consistency between correlation coefficients and the regressed terms from our algebraic basis function surrogates in Section S2. Calculation of Sobol sensitivity indices uses a specialized sampling scheme, which would normally require hundreds of thousands of **Prescient** simulations for our eight market parameters. Consequently, it is typical to use high-accuracy surrogates (e.g., high R^2) to facilitate the analysis [74]. We run Sobol sensitivity analysis using the high-accuracy neural network surrogates presented in Section 4.2.

We briefly describe the GSA methods here and refer the reader to more extensive literature on their derivation and applicability. For our purposes, we denote $X_i : i \in \{1, \dots, 8\}$ as random variables corresponding to the design inputs in Table 2 and $Y_j : j \in \{1, 2\}$ as the similar market outputs for revenue and the number of startups. We do not perform sensitivity analysis on the zone outputs from the table. We also note that our input variables are uncorrelated by design.

¹Corresponding author: adowling@nd.edu

S1.1. Calculating Correlation Coefficients

Correlation coefficients provide first-order information about relationships among variables. The Pearson correlation is given by (S1a), which measures the linear correlation between variables X_i and Y_j . A value of 0 implies no correlation between variables, and a value of -1 or 1 implies perfect positive or negative *linear* correlation. Within (S1a), $Cov(X_i, Y_j)$ represents the covariance between input variable X_i and output variable Y_j , σ_{X_i} is the standard deviation of X_i and σ_{Y_j} is the standard deviation of Y_j .

Eq. (S1b) corresponds to the Spearman rank correlation coefficient, which is the same as Pearson but instead measures the correlation between ranked variables (i.e., it maps observations in the data to integer ranks). The Spearman coefficient captures monotonic correlations instead of linear correlations and is less sensitive to outliers or long-tails in the data. The terms in (S1b) correspond to (S1a), but we use $R(\cdot)$ to denote the rank variables.

$$r_{X_i, Y_j}^p = \frac{Cov(X_i, Y_j)}{\sigma_{X_i} \sigma_{Y_j}} \quad (\text{S1a})$$

$$r_{X_i, Y_j}^s = \frac{Cov(R(X_i), R(Y_j))}{\sigma_{R(X_i)} \sigma_{R(Y_j)}} \quad (\text{S1b})$$

Eq. (S2a) denotes *partial* linear correlation coefficients between variables X_i and Y_j . The partial coefficient measures the linear strength and direction of the relationship between variables after removing other variable effects. Partial correlation coefficients can be calculated using linear regression residuals or inverse covariance matrices. We opt to show matrix inversion formulation here, and we refer the reader to (Seongho [75]) and (Whittaker [76]) for a more detailed derivation and explanation of partial correlation coefficients.

Given the vector V of random variables containing our 8 study inputs (X_1, X_2, \dots, X_8), we are interested in the partial correlation for each *individual* output. For each output we denote the vector V_{Y_j} as $(X_1, X_2, \dots, X_8, Y_j)$. We denote the covariance matrix for the vector V_{Y_j} as C_{Y_j} . We evaluate the inverse-covariance matrix $D_{Y_j} = C_{Y_j}^{-1}$ where the matrix elements d_{ij} correspond to the input variable X_i and the output variable Y_j . We can then evaluate the partial correlation of Y_j with respect to each X_i according to Eq. (S2a).

Eq. (S2b) calculates the ranked partial correlation coefficient using the same methodology as the partial correlation coefficient applied to the rank transformed variables. Here we use d_{ij}^R to denote rank-transformed variables to create the inverse-covariance matrix. The results of each correlation coefficient are shown in the heatmap in Figure S1.

$$r_{X_i, Y_j}^{pcc} = \frac{-d_{ij}}{\sqrt{(d_{ii})} \sqrt{(d_{jj})}} \quad (\text{S2a})$$

$$r_{X_i, Y_j}^{prcc} = \frac{-d_{ij}^R}{\sqrt{(d_{ii}^R)} \sqrt{(d_{jj}^R)}} \quad (\text{S2b})$$

S1.2. Variance-Based Sensitivity

We calculate Sobol sensitivity indices [74] for our study denoted by Eq. (S3) using the SALib [77] Python package. Sobol sensitivity indices quantify how much of the variance in model output is attributed to an

input. Inputs with a low sensitivity index contribute small variations to a model output whereas a high sensitivity index can significantly change the output.

The first-order Sobol sensitivity index S_{ij} is given by Eq. (S3a) and indicates the expected reduction in model variance when X_i is fixed. Here, $E(Y_j|X_i)$ denotes the expected value of the output Y_j when parameter X_i is fixed, and $Var(Y_j)$ is the total variance of Y_j . The total Sobol sensitivity index S_{ij}^T given by Eq. (S3b) includes the sensitivity of both first-order effects and interactions between X_i and all other parameters (e.g., second-order effects). Here, $E(Y_j|X_{\sim i})$ denotes that all uncertain parameters except X_i are fixed. Second-order (and higher-order) indices can be calculated similarly, but their formulations are not reported here.

$$S_{ij} = \frac{Var(E(Y_j|X_i))}{Var(Y_j)} \quad (\text{S3a})$$

$$S_{ij}^T = 1 - \frac{Var(E(Y_j|X_{\sim i}))}{Var(Y_j)} \quad (\text{S3b})$$

S1.3. Sensitivity Results

The full GSA results are reported in Tables S1, S2, and S3. With respect to correlation coefficients, revenue is most correlated with capacity (x_1) and marginal cost (x_6), and the number of startups is most correlated (negatively) with startup profile (x_8) and slightly correlated with marginal cost and the minimum startup time (x_4). The interpretation of other correlation coefficients does not change considerably from our Pearson results and shows that the correlations are either the same or stronger. Figure S1 shows heatmaps of our correlation results for different correlation coefficients.

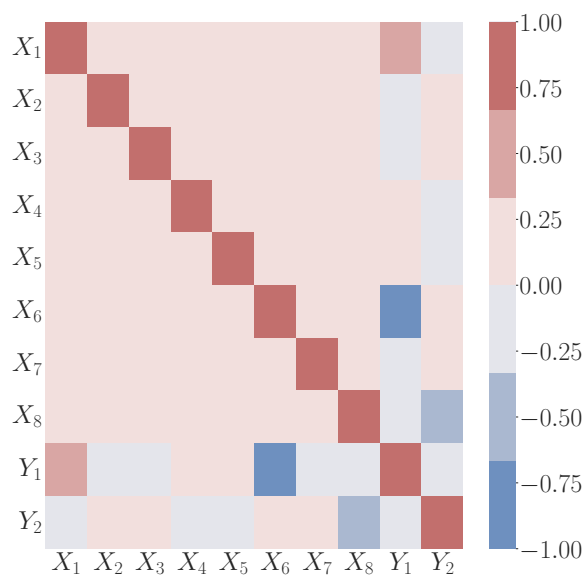
Table S2 reports the Sobol first-order and total effect indices obtained using our neural network surrogates. First-order Sobol indices sum to less than one (as expected), but the total effect indices here are higher because they include interaction effects. Our Sobol results are mostly consistent with our correlation coefficients but further help quantify each input’s importance. For instance, the marginal cost contributes the most variance to revenue (0.76) while P_{max} is a weaker effect (0.27). The Sobol indices also qualitatively verify our neural network surrogates; the other variables contribute much less variance compared to marginal cost and design capacity, which we observed in Figure 4. The number-of-startup sensitivities are also consistent with the sweep and correlation results. The startup profile explains the most variance, followed by marginal cost and minimum startup time.

Metric	X_1	X_2	X_3	X_4	X_5	X_6	X_7	X_8
r_{X_i, Y_1}^p	0.5	-0.02	-0.02	0.01	0	-0.7	-0.09	-0.08
r_{X_i, Y_1}^s	0.51	-0.02	-0.06	0	-0	-0.7	-0.08	-0.06
r_{X_i, Y_1}^{pcc}	0.71	0.35	0.35	0.013	-0.31	-0.81	-0.17	-0.17
r_{X_i, Y_1}^{prcc}	0.73	-0.039	-0.12	0.01	-0.002	-0.82	-0.16	-0.13
r_{X_i, Y_2}^p	-0.02	0.08	0.02	-0.17	-0.06	0.23	0.06	-0.62
r_{X_i, Y_2}^s	-0.02	0.22	0.06	-0.07	-0.03	0.3	0.17	-0.57
r_{X_i, Y_2}^{pcc}	-0.024	0.11	0.027	-0.23	-0.078	0.3	0.088	-0.65
r_{X_i, Y_2}^{prcc}	-0.029	0.29	0.083	-0.094	-0.036	0.39	0.23	-0.63

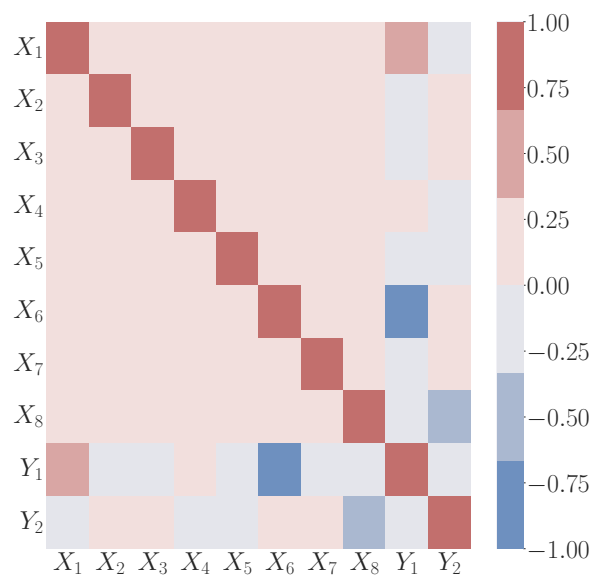
Table S1: Summary of global sensitivity analysis using Pearson, Spearman, partial correlation, and partially ranked correlation coefficients. The coefficients are tabulated for Y_1 (annual revenue) and Y_2 (annual number of startups) concerning each input variable.

Metric	X_1	X_2	X_3	X_4	X_5	X_6	X_7	X_8
S_{X_i, Y_1}	2.11e-01	2.50e-04	2.93e-04	-4.20e-04	9.96e-05	6.60e-01	4.81e-03	1.05e-02
S_{X_i, Y_1} (95% Conf)	1.12e-02	1.18e-03	5.17e-04	8.00e-04	6.40e-04	1.49e-02	3.10e-03	4.87e-03
S_{X_i, Y_1}^T	2.65e-01	3.29e-03	7.33e-04	1.59e-03	7.99e-04	7.67e-01	2.04e-02	6.45e-02
S_{X_i, Y_1}^T (95% Conf)	6.83e-03	2.35e-04	3.11e-05	9.57e-05	5.69e-05	1.60e-02	1.20e-03	3.29e-03
S_{X_i, Y_2}	4.68e-04	5.25e-03	1.28e-03	5.53e-02	1.07e-02	1.39e-01	4.83e-03	3.80e-01
S_{X_i, Y_2} (95% Conf)	8.41e-04	3.28e-03	1.11e-03	1.06e-02	6.09e-03	1.40e-02	5.41e-03	2.47e-02
S_{X_i, Y_2}^T	1.41e-03	3.30e-02	2.22e-03	2.43e-01	5.77e-02	3.56e-01	3.39e-02	7.66e-01
S_{X_i, Y_2}^T (95% Conf)	1.37e-04	2.62e-03	1.25e-04	1.19e-02	4.37e-03	1.58e-02	2.97e-03	3.01e-02

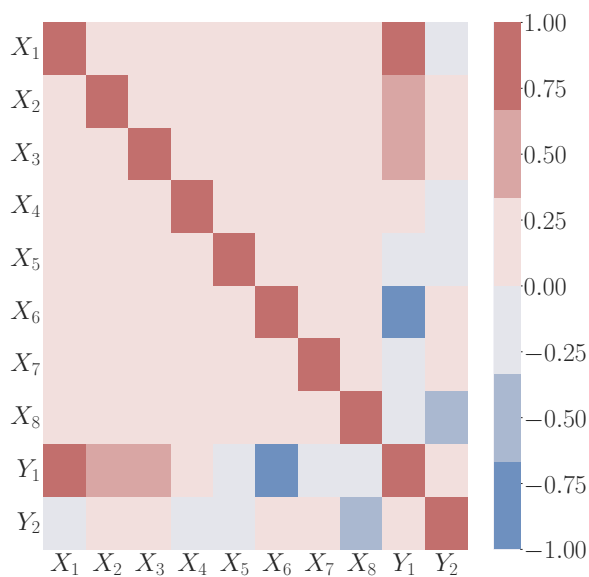
Table S2: First order and total order Sobol sensitivity indices with 95% confidence limits. The indices are tabulated for Y_1 (annual revenue) and Y_2 (annual number of startups) concerning each input variable.



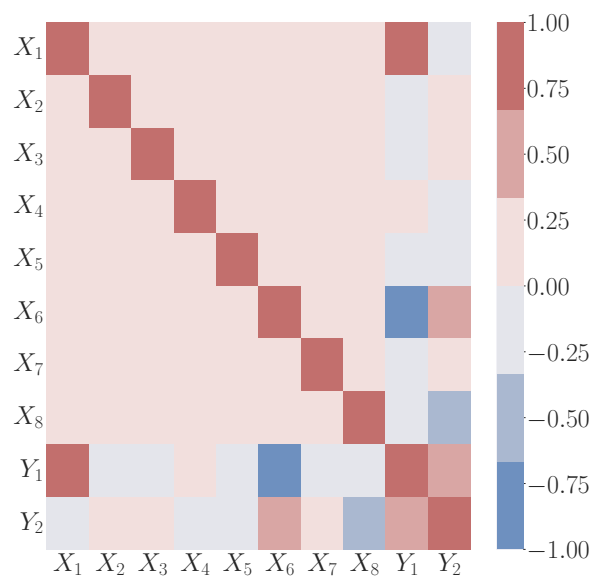
(a) Pearson



(b) Spearman



(c) PCC



(d) PRCC

Figure S1: Correlation coefficients among simulation inputs and outputs. The main manuscript contains variable definitions in Table 2. S1a: Pearson correlation coefficients. S1b: Spearman correlation coefficients, S1c: partial correlation coefficients, S1d partial ranked correlation coefficients.

Pair	$S^2_{X_{ij}, Y_1}$	$S^2_{X_{ij}, Y_1}$ 95% Conf	$S^2_{X_{ij}, Y_2}$	$S^2_{X_{ij}, Y_2}$ 95% Conf
X_1X_2	7.55e-04	1.59e-02	-4.69e-04	1.25e-03
X_1X_3	9.51e-04	1.59e-02	-6.20e-04	1.22e-03
X_1X_4	1.27e-03	1.57e-02	-6.02e-04	1.20e-03
X_1X_5	6.14e-04	1.58e-02	-7.09e-04	1.25e-03
X_1X_6	4.63e-02	1.49e-02	-3.35e-04	1.48e-03
X_1X_7	5.03e-04	1.55e-02	-6.01e-04	1.22e-03
X_1X_8	1.98e-03	1.53e-02	-2.57e-04	9.81e-04
X_2X_3	-2.19e-04	1.81e-03	-8.75e-04	5.28e-03
X_2X_4	-2.32e-04	1.81e-03	-4.73e-04	5.55e-03
X_2X_5	-2.53e-04	1.81e-03	-7.88e-05	5.33e-03
X_2X_6	4.38e-04	2.20e-03	1.70e-03	5.85e-03
X_2X_7	-3.65e-04	1.77e-03	-2.94e-04	5.07e-03
X_2X_8	7.33e-05	1.83e-03	1.18e-03	6.46e-03
X_3X_4	6.72e-05	9.20e-04	-8.51e-04	1.91e-03
X_3X_5	6.35e-05	9.21e-04	-8.74e-04	1.77e-03
X_3X_6	5.65e-05	9.01e-04	-6.56e-04	1.97e-03
X_3X_7	4.21e-05	9.00e-04	-6.24e-04	1.75e-03
X_3X_8	1.23e-04	8.54e-04	-1.17e-04	2.44e-03
X_4X_5	4.61e-04	1.21e-03	-4.47e-03	1.66e-02
X_4X_6	1.00e-03	1.19e-03	5.15e-05	1.83e-02
X_4X_7	4.07e-04	1.21e-03	-5.06e-03	1.72e-02
X_4X_8	5.72e-04	1.23e-03	1.22e-01	2.32e-02
X_5X_6	-1.27e-05	8.91e-04	-3.54e-04	9.39e-03
X_5X_7	-1.50e-04	9.02e-04	-3.77e-03	8.37e-03
X_5X_8	-1.46e-04	9.24e-04	2.41e-02	1.31e-02
X_6X_7	9.28e-03	2.37e-02	-2.31e-03	2.06e-02
X_6X_8	4.09e-02	2.53e-02	1.45e-01	2.43e-02
X_7X_8	1.55e-03	5.26e-03	9.58e-03	8.77e-03

Table S3: Second order Sobol sensitivities and 95% confidence limits. Notable interactions are X_1X_6 , X_6X_8 , X_4X_8 , and X_5X_8

S2. ALAMO Surrogate Models

$$Y_{revenue} = 0.502X1 - 0.022X2 - 0.025X3 - 0.031X4 - 0.028X5 - 0.698X6 - 0.101X7 - 0.084X8 + 0.037X1^2 + 0.049X2^2 + 0.048X3^2 + 0.043X4^2 + 0.075X5^2 - 0.344X6^2 + 0.065X7^2 \quad (S4)$$

$$Y_{startups} = 0.015X1 - 0.085X2 + 0.017X3 + 0.193X4 - 0.056X5 - 0.23X6 + 0.065X7 + 0.079X8 + 0.006X1^2 + 0.017X2^2 - 0.01X3^2 - 0.022X4^2 + 0.023X6^2 - 0.381X8^3 - 0.244X4X8 \quad (S5)$$

$$Y_{zone0} = -0.011X1 - 0.055X2 + 0.01X3 + 0.024X4 + 0.034X5 + 0.828X6 + 0.149X7 + 0.026X8 - 0.069X1^2 + 0.069X2^2 - 0.082X3^2 - 0.07X4^2 - 0.11X5^2 + 0.395X6^2 - 0.093X7^2 \quad (S6a)$$

$$Y_{zone1} = -0.021X1 - 0.207X2 - 0.06X3 + 0.054X4 + 0.012X5 - 0.122X6 - 0.191X7 - 0.109X8 + 0.071X1^2 + 0.277X2^2 - 0.123X3^2 + 0.073X4^2 + 0.103X5^2 + 0.355X2^3 + 0.131(X2X6)^2 \quad (S6b)$$

$$Y_{zone2} = -0.407X1 - 0.381X2 + 0.004X4 - 0.021X5 - 0.357X6 - 0.268X7 - 0.068X8 + 0.024X1^2 + 0.105X2^2 - 0.014X3^2 + 0.038X4^2 + 0.066X5^2 - 0.324X6^2 + 0.101X7^2 - 0.02X8^2 \quad (S6c)$$

$$Y_{zone3} = -0.028X1 - 0.045X2 - 0.214X3 - 0.043X4 - 0.013X5 + 0.022X6 - 0.075X7 - 0.246X8 + 0.02X1^2 - 0.724X3^2 - 0.259X6^2 + 0.126X8^2 - 0.111X6^3 + 0.023X1X3 + 0.839 \quad (S6d)$$

$$Y_{zone4} = -0.179X1 - 0.075X2 - 0.078X4 - 0.016X5 - 0.104X6 - 0.283X8 + 0.01X1^2 + 0.023X2^2 - 0.018X3^2 + 0.016X4^2 + 0.018X5^2 - 0.228X6^2 + 0.624X8^2 - 0.033X2^3 - 0.451(X3X8)^2 \quad (S6e)$$

$$Y_{zone5} = -0.404X1 - 0.408X2 - 0.122X3 + 0.061X4 + 0.011X5 - 0.387X6 - 0.227X7 - 0.04X8 + 0.018X1^2 + 0.051X2^2 + 0.173X3^2 - 0.019X4^2 - 0.003X5^2 - 0.259X6^2 + 0.04X7^2 \quad (S6f)$$

$$Y_{zone6} = -0.021X1 - 0.033X2 - 800.305X3 + 0.002X6 - 0.065X7 - 0.158X8 - 0.01X1^2 + 0.028X2^2 + 0.298X3^2 - 0.239X6^2 - 0.026X8^2 + 533.854X3^3 - 0.122X6^3 - 0.029X8^3 + 0.107X1X3 \quad (S6g)$$

$$Y_{zone7} = -0.424X1 - 0.37X2 - 0.113X3 + 0.043X4 - 0.005X5 - 0.526X6 - 0.209X7 - 0.016X8 + 0.039X1^2 + 0.052X2^2 + 0.089X3^2 + 0.004X4^2 + 0.035X5^2 - 0.289X6^2 + 0.056X7^2 \quad (S6h)$$

$$Y_{zone8} = -0.057X1 - 0.094X2 - 0.259X3 - 0.097X4 - 0.055X5 - 0.226X6 - 0.074X7 - 0.233X8 + 0.086X1^2 + 0.098X2^2 - 0.27X3^2 + 0.075X4^2 + 0.119X5^2 - 0.149(X3X6)^2 + 0.103(X3 * X8)^3 \quad (S6i)$$

$$Y_{zone9} = -0.407X1 - 0.378X2 - 0.07X3 + 0.019X4 - 0.018X5 - 0.547X6 - 0.215X7 - 0.014X8 - 0.01X1^2 + 0.074X2^2 - 0.019X3^2 + 0.028X4^2 + 0.067X5^2 - 0.247X6^2 + 0.081X7^2 \quad (S6j)$$

$$Y_{zone10} = -0.041X1 - 0.035X2 - 0.033X3 + 0.032X4 - 0.026X5 - 0.912X6 - 0.072X7 - 0.032X8 - 0.042X1^2 + 0.045X2^2 + 0.054X3^2 + 0.042X4^2 + 0.07X5^2 + 0.333X6^2 - 0.054X7^2 \quad (S6k)$$

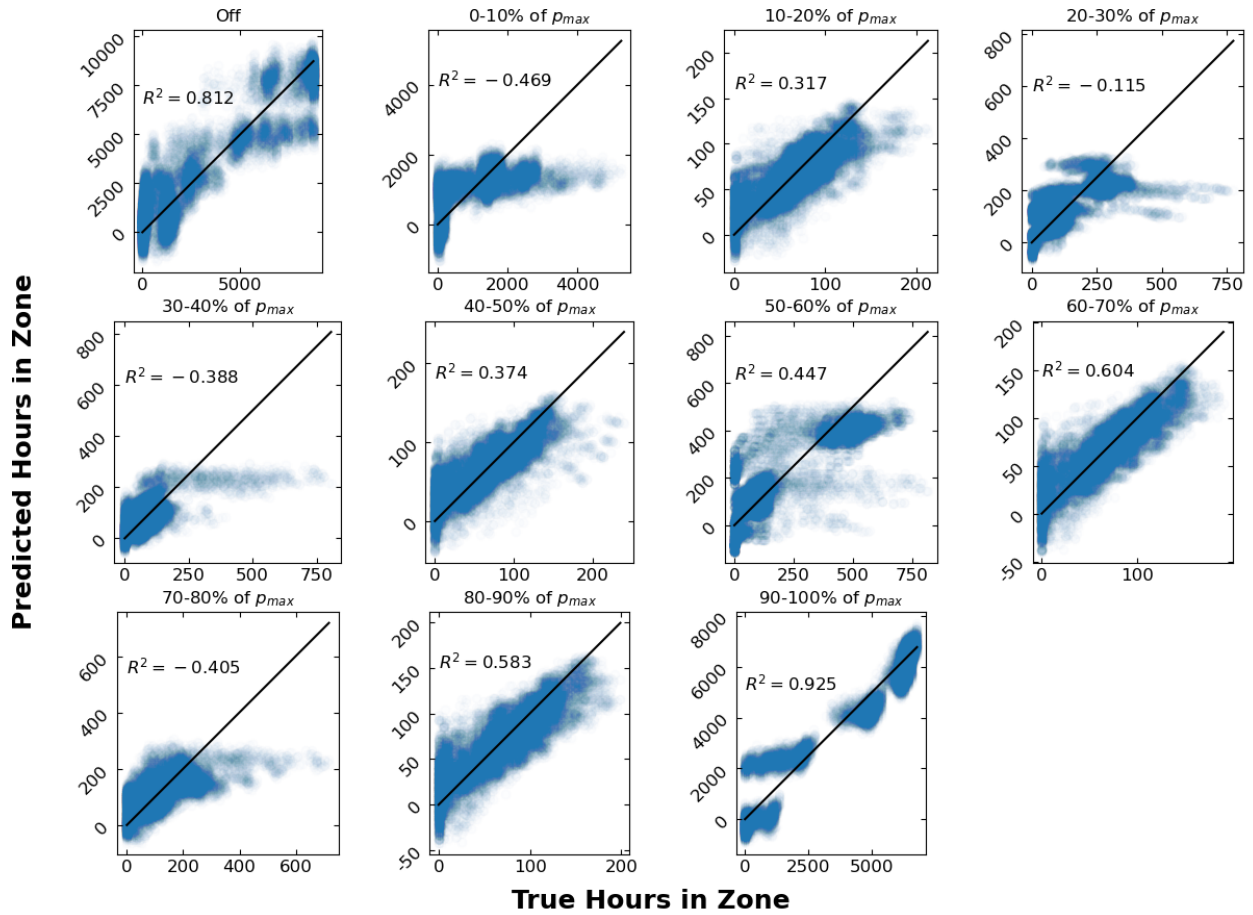


Figure S2: Test-set parity plots and accuracy for ALAMO zone surrogates. Each subfigure corresponds to an individual zone surrogate.

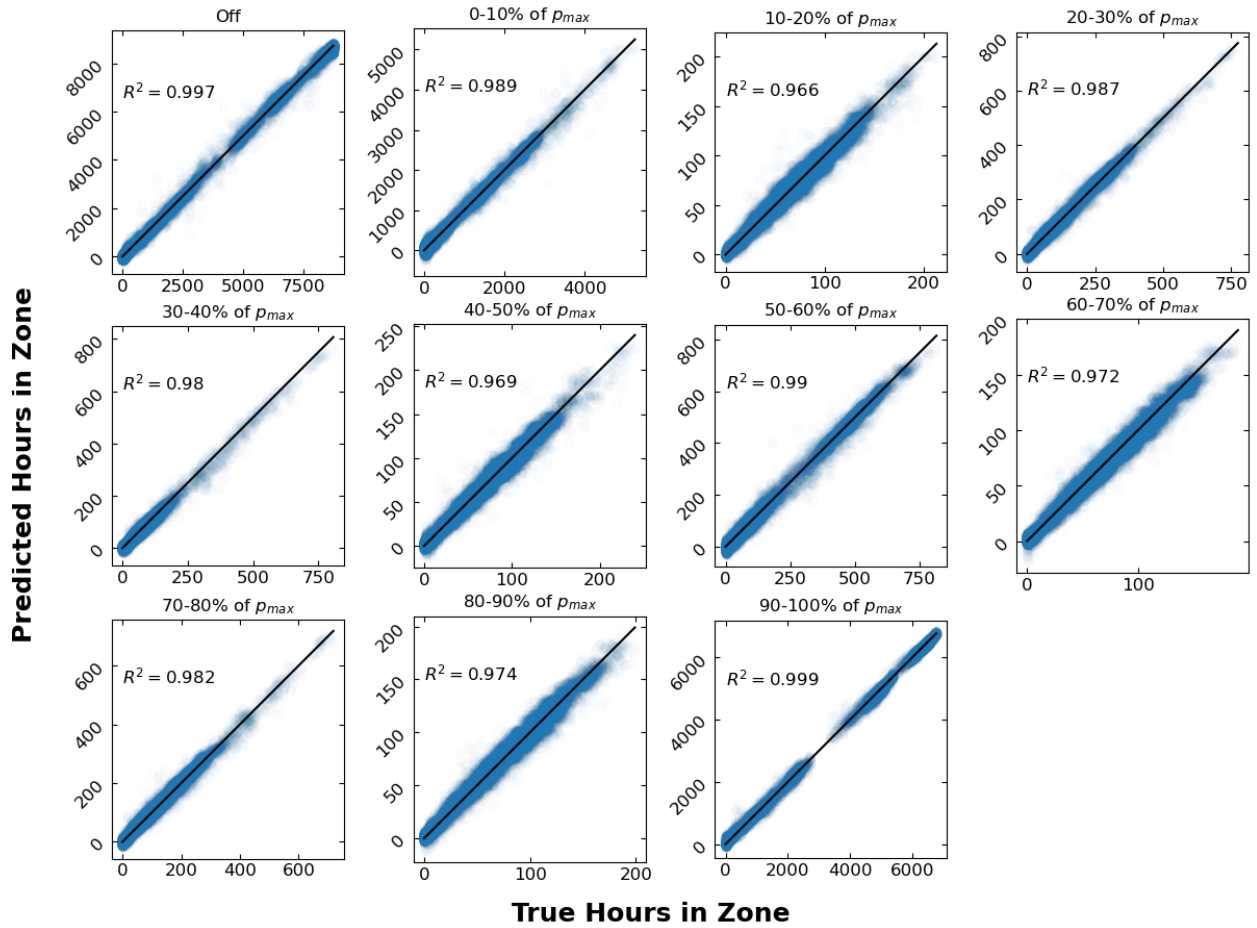


Figure S3: Test-set parity plots and accuracy for the NN zone surrogate. Each subfigure corresponds to one of the NN outputs.

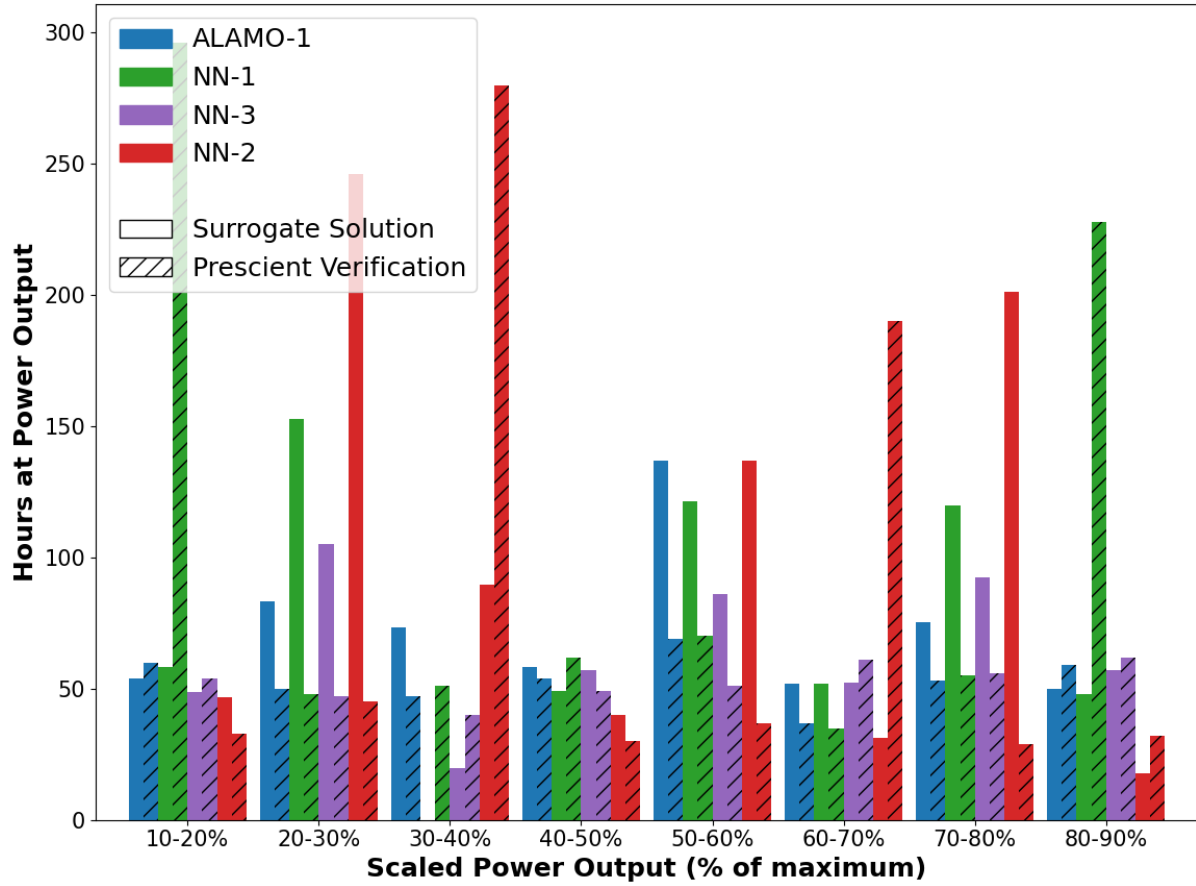


Figure S4: Surrogate design verification for intermediate-zone power outputs. Bars correspond to the settings defined in Table 6 in the main manuscript. Solid bars are surrogate model predictions and hashed bars are the corresponding simulated values from Prescient.

S3. Case Study Energy System Performance and Cost Correlations

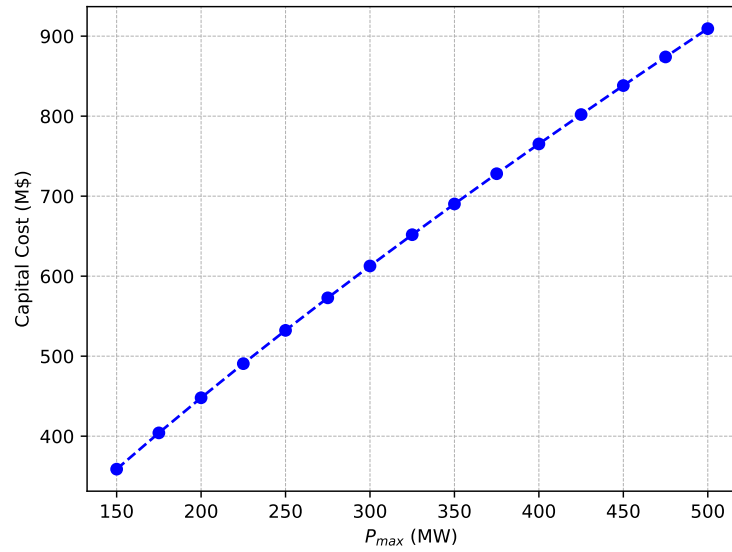


Figure S5: Capital cost vs. maximum power capacity for the steam generator. The costing correlations have been extrapolated to lower capacities of less than 300 MW for this illustrative case study.

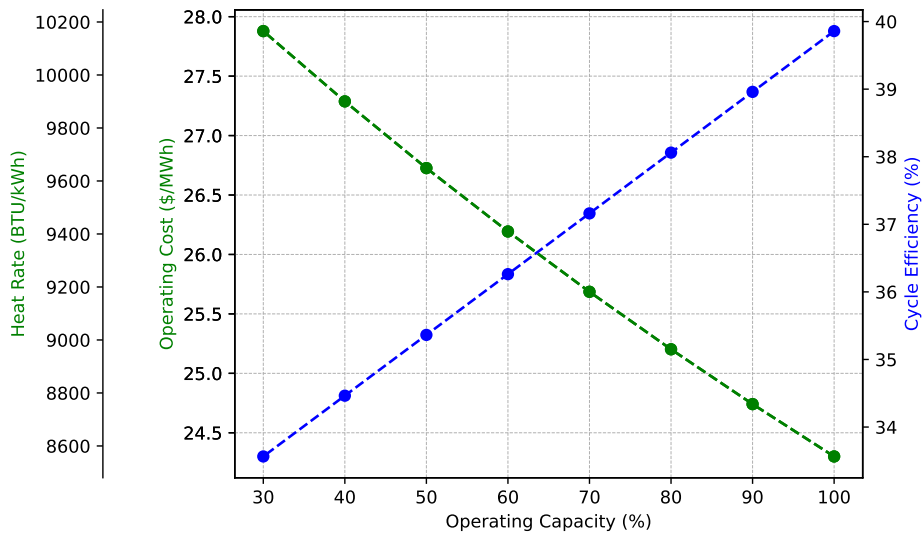


Figure S6: Heat rate, operating cost, and cycle efficiency vs. operating capacity for the steam generator. At the maximum power output, the cycle efficiency is maximized and the specific operating cost is minimized.

S4. RTS-GMLC Grid Capacity Factor Distribution

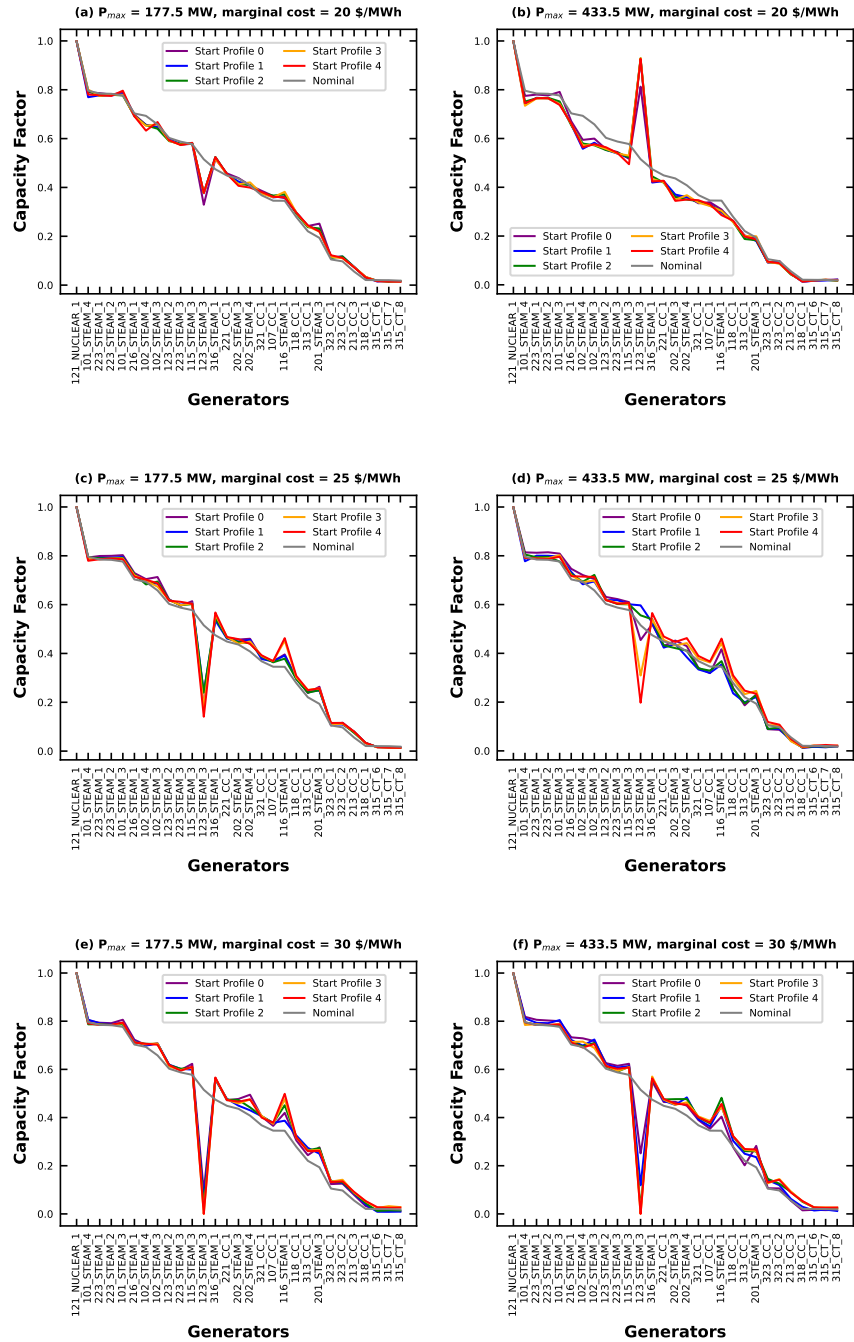


Figure S7: Capacity Factor distribution in the energy grid (RTS-GMLC). The figure only shows generators with nominal capacity factors of 5 % and above; generators with lower capacity factors are dropped off. P_{max} and marginal cost (MC) values are for the perturbed generator, 123-STEAM-3. The results on this figure correspond to **Prescient** simulation results on Figure

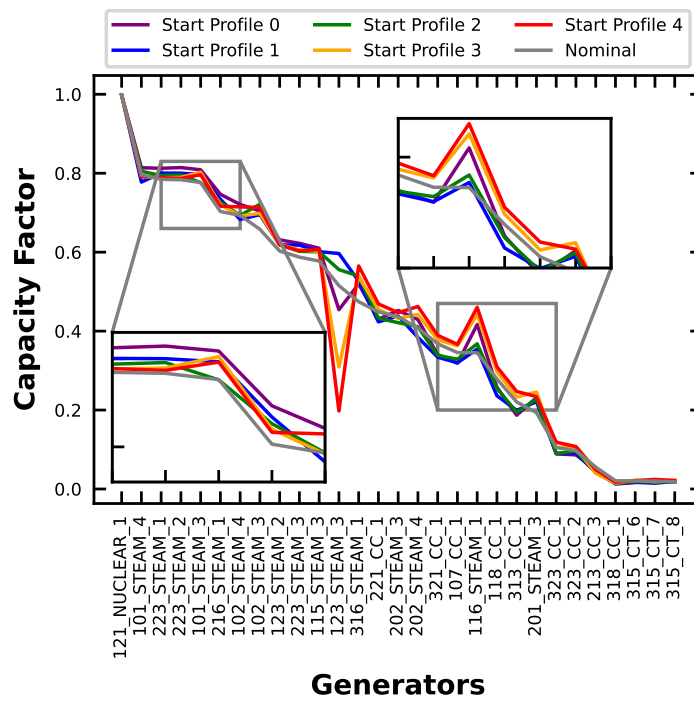


Figure S8: Capacity Factor distribution with zoom-in views to emphasize trends. Generator 123-STEAM-3 parameters: P_{max} = 433 MW, marginal cost = 25 \$/MWh